Bioactive Materials 21 (2023) 142–156

Contents lists available at ScienceDirect

Bioactive Materials

journal homepage: www.keaipublishing.com/en/journals/bioactive-materials

Growth and differentiation of human induced pluripotent stem cell (hiPSC)-derived kidney organoids using fully synthetic peptide hydrogels

Niall J. Treacy [a,b,1], Shane Clerkin [a,b,1], Jessica L. Davis [a,b], Ciarán Kennedy [a,b], Aline F. Miller [c], Alberto Saiani [c], Jacek K. Wychowaniec [d,2], Dermot F. Brougham [d], John Crean [a,b,*]

[a] Diabetes Complications Research Centre, University College Dublin (UCD) Conway Institute of Biomolecular and Biomedical Research and Belfield, Dublin 4, Ireland
[b] UCD School of Biomolecular and Biomedical Science, Belfield, Dublin 4, Ireland
[c] Department of Materials & Manchester Institute of Biotechnology (MIB), School of Natural Sciences, Faculty of Science and Engineering, The University of Manchester, UK
[d] UCD School of Chemistry, University College Dublin, Belfield, Dublin 4, Ireland

ARTICLE INFO

Keywords:
Human kidney organoids
Fully synthetic matrices
Self-assembling peptide hydrogels
Single-cell RNA sequencing

ABSTRACT

Human induced pluripotent stem cell (hiPSC)-derived kidney organoids have prospective applications ranging from basic disease modelling to personalised medicine. However, there remains a necessity to refine the biophysical and biochemical parameters that govern kidney organoid formation. Differentiation within fully-controllable and physiologically relevant 3D growth environments will be critical to improving organoid reproducibility and maturation. Here, we matured hiPSC-derived kidney organoids within fully synthetic self-assembling peptide hydrogels (SAPHs) of variable stiffness (storage modulus, G′). The resulting organoids contained complex structures comparable to those differentiated within the animal-derived matrix, Matrigel. Single-cell RNA sequencing (scRNA-seq) was then used to compare organoids matured within SAPHs to those grown within Matrigel or at the air-liquid interface. A total of 13,179 cells were analysed, revealing 14 distinct clusters. Organoid compositional analysis revealed a larger proportion of nephron cell types within Transwell-derived organoids, while SAPH-derived organoids were enriched for stromal-associated cell populations. Notably, differentiation within a higher G' SAPH generated podocytes with more mature gene expression profiles. Additionally, maturation within a 3D microenvironment significantly reduced the derivation of off-target cell types, which are a known limitation of current kidney organoid protocols. This work demonstrates the utility of synthetic peptide-based hydrogels with a defined stiffness, as a minimally complex microenvironment for the selected differentiation of kidney organoids.

1. Introduction

Human embryonic [1] and induced pluripotent stem cells (hiPSCs) [2] have facilitated ground-breaking advancements in the field of regenerative medicine in recent years, including the directed differentiation of numerous three-dimensional (3D) organotypic structures *in vitro* [3–7]. These self-organising, heterogeneous cellular aggregates, termed organoids, have been shown to closely approximate structural and functional features of their respective *in vivo* counterparts and represent a novel means to study human development and disease [8,9]. Organoids may also circumvent existing pre-clinical caveats and improve early drug development attrition rates by serving as a suitable human tissue model for pharmacological and toxicological screening strategies [10–12]. Ultimately, stem cell-derived organoids may facilitate the generation of personalised and immuno-compatible replacement tissues for patients.

Considering its remarkable anatomical complexity and the current paucity of effective treatment options for patients with chronic kidney disease (CKD), the generation of stem cell-derived kidney organoids has been a particularly exciting breakthrough in recent years [6,8,13–18]. Recent advances have been guided by an improved understanding of renal specification *in vivo,* including initial mesodermal patterning and

Peer review under responsibility of KeAi Communications Co., Ltd.
* Corresponding author. UCD School of Biomolecular and Biomedical Science, Belfield, Dublin 4, Ireland.
E-mail address: john.crean@ucd.ie (J. Crean).
[1] These authors contributed equally to this work.
[2] Current address: AO Research Institute Davos, Clavadelerstrasse 8, 7270, Davos, Switzerland.

https://doi.org/10.1016/j.bioactmat.2022.08.003
Received 21 December 2021; Received in revised form 27 June 2022; Accepted 1 August 2022

subsequent induction of the two primary kidney progenitors, the ureteric bud and the metanephric mesenchyme. Guided by an understanding of normal developmental processes, current stem cell-derived kidney organoid culture methods induce renal cell fate trajectories by temporal addition of exogenous growth factors and small molecules to ultimately give rise to collecting duct and segmented nephron structures [6].

Precise control of exogenous morphogens to induce renal developmental signalling pathways and subsequent self-organisation is a common feature of current stem cell-derived kidney organoid protocols. Indeed, alterations to the timing and concentrations of certain small molecules has been shown to affect anterior and posterior patterning and hence the proportions of renal cell types generated *in vitro* [6]. However, both the biochemical and the biophysical properties of the cellular microenvironment are known to influence tissue growth and morphogenesis (reviewed in Refs. [19–22]). Consequently, biomaterials have increasingly been introduced to a variety of culture systems to more readily control the bio-interface and investigate how chemical and mechanical parameters influence developmental processes [5,23–27].

Self-assembling peptide hydrogels (SAPHs) represent a particularly advantageous class of synthetic biomaterial for prospective cell culture, regenerative medicine and drug discovery applications [28,29]. In nature, the process of self-assembly occurs due to the spontaneous, non-covalent association of molecules into well-ordered and structurally stable configurations. Inspired by this hierarchical organisation, artificial amphipathic peptides have been designed to undergo spontaneous self-assembly into β-sheet rich fibrillar structures in aqueous solution. These flexible nanofibres subsequently associate and entangle when above a critical concentration to form physical hydrogels with architecture and properties analogous to native ECM [30,31]. Interestingly, the resulting peptide hydrogels combine the favourable properties of both natural and synthetic matrices; the peptide sequences are composed of naturally occurring amino acids that may be reproducibly chemically formulated, and their spontaneous self-assembly obviates the requirement for chemical cross linkers. Moreover, due to their composition, peptide degradation generates amino acid products that are physiologically metabolised [32]. Additionally, the mechanical properties of peptide hydrogels can be easily altered by modifying parameters including peptide concentration, amino acid sequence and solvent electrolyte ion composition [31,33]. Considering their ECM-like configuration, inherent biocompatibility, physical tunability and reproducible preparation, SAPHs have already been utilised for a variety of applications including drug delivery and tissue engineering strategies [34–36].

In this work, we describe the growth, differentiation, maintenance, and characterisation of hiPSC-derived kidney organoids within fully synthetic SAPHs. We first aimed to address limitations associated with current kidney organoid differentiation protocols which either do not utilise support matrices [6,13] or rely on poorly reproducible animal-derived materials, such as Matrigel [14], as extracellular scaffolds for differentiation. The effect of hydrogel stiffness on cell differentiation was subsequently investigated using two SAPHs of varying mechanical strengths. Similarities and differences between constituent organoid cell types within the two synthetic hydrogels were compared to organoids grown in an air-liquid interface (Transwell) or Matrigel-supported organoids using single-cell RNA sequencing (scRNA-seq). This work highlights the potential of SAPHs as physiologically relevant, 3D support matrices for the derivation of hiPSC-derived kidney organoids.

2. Materials and methods

2.1. Self-assembling peptide hydrogels

Synthetic SAPHs were obtained from Manchester BIOGEL (Alderley Edge, UK), and used as received. Two mechanically distinct hydrogels were used in this study, both characterised by the same high positive charge when maintained at physiological pH: PeptiGel Alpha4 (low stiffness) and PeptiGel Alpha5 (high stiffness).

2.2. Oscillatory rheology

Rheological studies were performed using the MCR301 rheometer (Anton Paar). Parallel plate geometry with a 25 mm diameter top plate and 0.25 mm gap was used. 300 μL of hydrogel samples were preconditioned in 1 mL STEMdiff APEL 2 Medium (StemCell Technologies) containing 1% Antibiotic-Antimycotic (100X) (Gibco) and 5% PFHM-II Protein-Free Hybridoma Medium (Gibco) for 1 h (day 0) or 15 days ± kidney organoids. Medium was changed at timepoints corresponding to changes in the kidney organoid differentiation protocol (Fig. 1B). Day 15 represents the maximum duration of organoid encapsulation within the respective hydrogels. Samples were maintained at 37 °C, in a 95% air and 5% CO_2 environment. For measurements, 300 μL of sample was placed on the bottom stationary plate using a spatula, with the top oscillating plate lowered slowly to minimize hydrogel disruption. To measure samples following organoid exposure for 15 days, organoids were first excised using an 18-gauge needle. The sample was allowed to equilibrate at 37 °C for 3 min. The mechanical properties of the hydrogels were recorded by performing frequency sweeps from 0.1 to 15 Hz at 0.2% strain within the linear viscoelastic regime of the samples at 37 °C (as shown in (Fig. S1A). Presented values are shown as mean ± SD from frequency sweeps at 6.13 rad s^{-1}. For rheological experiments, minimum n = 3 of PeptiGels Alpha4 and Alpha5 were taken from multiple purchased batches.

2.3. Swelling test

Alpha4 and Alpha5 swelling ± kidney organoid was measured over 15 days with medium changed at timepoints corresponding to changes in the kidney organoid differentiation protocol (Fig. 1B). Samples were prepared on sterile coverslips of known weights. Samples were weighed in a sterile environment pre-medium exposure, and at 1 h (day 0), day 3, day 7 and day 15 timepoints. The percentage swelling was calculated by: $\%S = (w_1/w_0)$ x 100, where w_1 is the weight at each timepoint and w_0 is sample weight pre-medium exposure. Minimum n = 3 of Alpha4 and Alpha5 from multiple purchased batches were used for measurements.

2.4. Transmission electron microscopy (TEM)

For TEM of the peptide hydrogels, samples were diluted (1:40) in ddH_20 to visualise individual peptide fibres. A carbon-coated copper 200 mesh grid (Electron Microscopy Sciences) was first placed on 10 μL of sample for 1 min, 10 μL of ddH_2O for 10 s and 10 μL 1% uranyl acetate solution for 30 s. Grids were then washed by placing the samples on to 10 μL ddH_2O for 10 s. Excess liquid was drained off with lint-free tissue after each step. The grid was allowed to dry at room temperature before imaging using the FEI Tecnai F12 TEM at 120 kV. Nanofibre width was quantified using ImageJ [37] by measuring ten fibre points per TEM micrograph.

For TEM of day 24 kidney organoids, samples were fixed in 2% paraformaldehyde (Electron Microscopy Sciences) and 2.5% glutaraldehyde (Sigma-Aldrich) in 0.1 M Sorensen's buffer overnight at 4 °C. Samples were post-fixed in 1% osmium tetroxide (OsO_4) in 0.1 M Sorensen's buffer and subsequently in 1% tannic acid (Sigma-Aldrich) in 0.1 M Sorensen's buffer. Each of the post-fixation incubations were carried out for 1 h at room temperature. 20 min (x3) 0.1 M Sorensen's buffer washes were performed prior to and between all post-fixation steps. Dehydration in 70% (10 min), 90% (10 min), 100% ethanol (20 min x3) and acetone (15 min x2) was then performed. Samples were incubated overnight in acetone:epon resin (50:50) at room temperature prior to polymerisation in epon resin at 60 °C overnight. The Leica EM UC7 ultramicrotome was then used to obtain ultra-thin sections (80 nm)

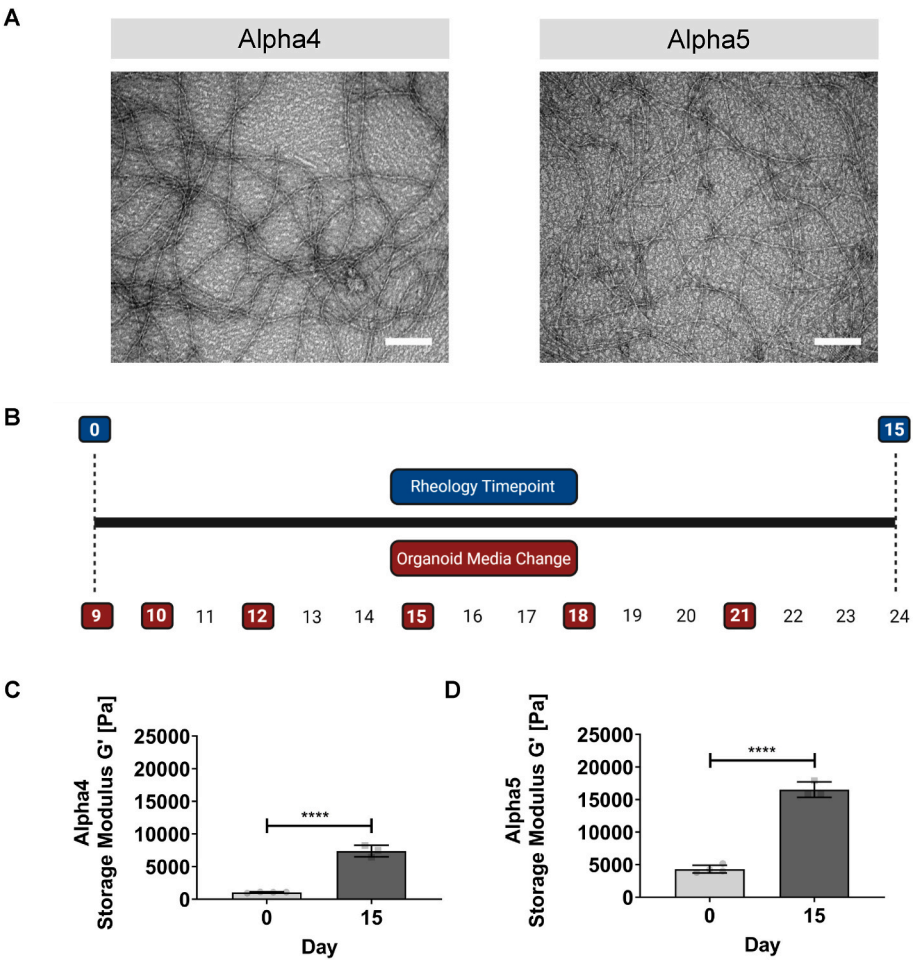

Fig. 1. Microstructural and mechanical characterisation of SAPHs Alpha4 and Alpha5. A) TEM micrographs of Alpha4 and Alpha5 showed peptide nanofibre networks that mimic *in vivo* fibrillar extracellular matrix architecture. 135000x, scale bar = 100 nm. **B)** Using oscillatory rheology, the mechanical stiffness (Storage Modulus, G′) of the SAPHs was investigated over a 15-day period with day 0 equating to the point of encapsulation on day 9 of the kidney organoid protocol. Days in red represent media changes that correspond to timepoints in the organoid protocol. Days in blue represent rheology measurement timepoints. **C)** Alpha4 and **D)** Alpha5 showed an increase in G′ over time. Measurements (minimum n = 3 from multiple purchased batches of hydrogel) were taken at 37 °C, with data expressed as mean ± SD; **** for $p < 0.0001$.

that were collected on carbon-coated copper grids. 2% uranyl acetate (20 min) and 3% lead citrate (5 min) were used for post-staining of samples. Sections were imaged using the FEI Tecnail2 BioTwin TEM at 120 kV.

2.5. Mass spectroscopy

Alpha4 and Alpha5 mass spectroscopy (MS) analysis ± kidney organoid was measured on day 0 and day 15 with medium changed at timepoints corresponding to changes in the kidney organoid differentiation protocol (Fig. 1B). To measure samples following organoid exposure for 15 days, organoids were first excised using a 18-gauge needle. Samples were diluted 1:20 and subsequently 1:640 in 80% Optima LC/MS Grade H_2O/20% Optima LC/MS Grade acetonitrile (both Thermo Fisher Scientific) with 0.1% formic acid (Merck). Analysis was carried out using an Agilent 6546 QTOF Mass Spectrometry system equipped with an Agilent 1260 Infinity Prime II LC system. Initial chromatographic conditions for sample introduction used a flow rate of 0.6 mL/min with 90% H_2O with 0.1% LC/MS formic acid, 10% CHROMASOLV LC/MS grade acetonitrile (Honeywell), with a linear gradient increase to 90% acetonitrile over 5 min and held isocratically at 90% for another 5 min. A post-run delay of 3 min was used to allow equilibration before the next sample. Injection volumes of 0.5 μL and 4 μL were used. A Zorbax Eclipse Plus C18 RRHD 2.1 × 50 mm, 1.8 μm LC column was used to effect chromatographic separation. MS acquisition was carried out on an Agilent 6546 system equipped with an AJS (Agilent Jet Stream) ESI source. Source conditions were: Drying gas temperature 325 °C at 8 L/min, Sheath gas 350 °C at 11 L/min, Capillary Voltage 4000 V, Nozzle voltage 2000 V, Fragmentor voltage 175 V. Data analysis was carried out using Agilent MassHunter Qualitative Analysis 10.0 software. Extracted Ion Chromatograms (EICs) were generated by combining the [M+H]+ and [M+Na]+ isotope series of both measured peptides.

2.6. Maintenance of hiPSCs

The human induced pluripotent stem cell (hiPSC) line HPSI1213i-babk_2 was obtained from the Wellcome Trust Sanger Institute in Cambridge, UK and was used for all experiments. hiPSCs were maintained in Essential 8™ Flex Medium (Gibco) in 6-well tissue culture plates coated with 10 μg/mL Vitronectin XF (StemCell Technologies) in a 37 °C incubator containing 95% air 5% CO_2. hiPSCs were passaged at 70% confluency using ReLeSr™ (StemCell Technologies). Essential 8™ Flex Medium was supplemented with Y-27632, a specific Rho-associated, coiled-coil containing protein kinase (ROCK) Inhibitor (10 μM) (Tocris) for 24 h following passaging.

2.7. Kidney organoid differentiation

hiPSCs were differentiated using a modified version first described by Takasato and colleagues [6]. Briefly, hiPSCs were seeded on 10 μg/mL Vitronectin XF-coated 6-well tissue culture plates at a density of 15,000 cells/cm^2 with Essential 8™ Flex Medium supplemented with 10 μM Y-27632. Cells were placed in a 37 °C, 95% air 5% CO_2 incubator for overnight culture. Monolayer cells were differentiated using STEMdiff APEL 2 Medium containing 1% Antibiotic-Antimycotic (100X) and 5% PFHM-II Protein-Free Hybridoma Medium (basal medium) supplemented with 8 μM CHIR99021 (Sigma-Aldrich). Medium was replenished after 48 h. On day 3, culture medium volume was doubled and

changed to basal medium supplemented with 200 ng/mL Recombinant Human Fibroblast Growth Factor 9 (FGF9) (Peprotech) and 1 μg/mL Heparin (Sigma-Aldrich). Medium was replenished every 48 h. On day 7, spent medium was removed and monolayer cells were incubated with basal medium containing 5 μM CHIR99021 for 1 h in a 37 °C, 95% air 5% CO_2 incubator. Cells were then washed with DPBS (Gibco) and incubated for 3 min in 0.05% Trypsin-EDTA (Gibco) to detach cells. Trypsin was neutralised with DMEM, low glucose, GlutaMAX™ Supplement, pyruvate (Gibco) supplemented with 10% (v/v) fetal bovine serum and 100 U/mL of penicillin, 100 μg/mL streptomycin (both Gibco). Cells were subsequently centrifuged at 400 *g* for 3 min at room temperature and re-suspended in basal medium containing 200 ng/mL FGF9 and 1 μg/mL Heparin. A cell count was performed and suspensions containing 500,000 cells were centrifuged in 1.5 mL microcentrifuge tubes at 400 *g* for 2 min at room temperature, with 180° rotations (x4 times) to generate compacted pellets of cells. Pellets were either transferred to 96-well Clear Round Bottom Ultra-Low Attachment Microplates (Corning) or placed on Transwell inserts with basal medium containing 200 ng/mL FGF9 and 1 μg/mL Heparin. On day 9, aggregates in ultra-low attachment plates were encapsulated within PeptiGel Alpha4, PeptiGel Alpha5 or Matrigel® Basement Membrane Matrix (LDEV-free, Corning). Aggregates were transferred to 12-well tissue culture plates using wide bore p200 pipette tips. Excess media was removed, and encapsulation was carried out by pipetting 100 μL of PeptiGel or Matrigel adjacent to the aggregate causing the pellet to be drawn into the hydrogel. Hydrogels containing organoids were maintained on the surface of the 12-well plate for the duration of the differentiation. PeptiGels were handled using a positive displacement pipette. Encapsulated aggregates were cultured in basal medium containing 200 ng/mL FGF9 and 1 μg/mL Heparin. Medium was replenished on day 10. On day 12, culture medium was switched to basal medium only. Medium was then replenished every 2–3 days until day 24.

2.8. Organoid viability assay

On day 24 of differentiation, viability of encapsulated organoids was assessed using the Invitrogen™ LIVE/DEAD Assay. Organoids were washed with DPBS three times (3 × 5 min) on a rocker at room temperature. Organoids were incubated with 2 μM Calcein-AM (live) and 2 μM ethidium-homodimer-1 (dead) for 30 min, protected from light, at 37 °C in a 95% air and 5% CO_2 incubator. Organoids were then washed with DPBS three times, with the final wash lasting 15 min on a rocker at room temperature. Images were acquired with the Axiovert 200 M microscope with an Andor iXon EMCCD camera. For this assay, encapsulated organoids were differentiated on μ-Dish 35 mm, polymer coverslip-bottom dishes (Ibidi) to facilitate subsequent imaging. Quantification of viability was calculated on ImageJ using the live or dead Integrated Density value (product of area and mean grey value) per organoid and expressing this as a percentage of the live plus dead Integrated Density value.

2.9. Immunofluorescence

On day 24 of differentiation, organoids were washed once with DPBS and fixed with 2% paraformaldehyde for 1 h at 4 °C. Organoids were subsequently washed twice with ice-cold DPBS and cryo-protected with a sucrose (Sigma-Aldrich) gradient; 10% (w/v) for 2 h at 4 °C, 15% (w/v) for 3 h at 4 °C and 30% (w/v) overnight at 4 °C. Organoids were then embedded in a 7.5% (w/v) type A gelatin (Sigma-Aldrich) 10% (w/v) sucrose solution, frozen in an ice-cold isopropanol bath and stored at −80 °C. Organoids were cut into 14 μm sections using the Leica CM1860 UV cryostat and stored at −80 °C on SuperFrost Plus™ Adhesion slides (Thermo Fisher Scientific) until required. For immunostaining, sections were traced with a 1 mm Edge Hydrophobic Barrier PAP Pen (Vector Laboratories) and re-hydrated/blocked with 5% goat serum (Sigma-Aldrich), 0.06% Triton X-100 (Sigma-Aldrich) in DPBS (blocking buffer) for 1 h. Sections were incubated with the primary antibodies diluted in blocking buffer overnight at 4 °C, then washed with DPBS three times. Sections were incubated with secondary antibodies and Hoechst 33342, Trihydrochloride, Trihydrate (Invitrogen) diluted in DPBS containing 5% goat serum overnight at 4 °C, then washed with DPBS three times. Biotinylated antibodies were additionally blocked using the Streptavidin/Biotin Blocking Kit (Vector Laboratories). DyLight® 649 Streptavidin secondary (Vector Laboratories) was diluted in DPBS and incubated for 15 min at room temperature. SlowFade Gold Antifade Reagent (Life Technologies) was added to slides prior to the addition of cover slips. For monolayer characterisation, hiPSCs were seeded and differentiated on Vitronectin-XF-coated μ-Slide 8 well dishes (Ibidi) or on glass coverslips and stained *in situ*, as above. Cells stained for Brachyury were blocked using donkey serum (Sigma-Aldrich). For wholemount immunofluorescence, organoids were processed in 48-well plates. Organoids were blocked for 2 h, with subsequent washes lasting 1 h using 0.1% Triton X-100 in DPBS. Organoids were cleared with a previously developed method using 60% (v/v) glycerol (Sigma-Aldrich) and 2.5 M fructose (Sigma-Aldrich) in ddH_2O [38] and imaged in μ-Slide 8 well dishes.

Primary antibodies include: Oct 3/4 (Santa Cruz, sc-5279, 1:300, secondary antibody 1:500), E-Cadherin (ECAD) (BD Biosciences, 610181, 1:300, secondary antibody 1:500), Brachyury (T) (R&D Systems, AF2085-SP, 1:100, secondary antibody 1:200), N-Cadherin (BD Biosciences, 610920, 1:300, secondary antibody 1:500), HOXD11 (Sigma-Aldrich, SAB1403944-100UG, 1:300, secondary antibody 1:500), Pax2 (Invitrogen, PA5-81235, 1:300, secondary antibody 1:500), LTL (Vector Laboratories, B-1325, 1:200, secondary antibody 1:400), WT1 (Santa Cruz, sc-7385, 1:100, secondary antibody 1:300), Laminin (Sigma-Aldrich, L9393, 1:300, secondary antibody 1:500), ZO-1 (Invitrogen, 61–7300, 1:300, secondary antibody 1:500), MEIS1/2/3 (Santa Cruz, sc-101850, 1:100, secondary antibody 1:200), αSMA (Sigma-Aldrich, A2547, 1:300, secondary antibody 1:500), NPHS2 (podocin) (Sigma-Aldrich, P0372, 1:300, secondary antibody 1:500), SIX2 (Proteintech, 11562-1-AP, 1:300, secondary antibody 1:500), F-Actin (Invitrogen Rhodamine phalloidin, R415, 1:200). Images were acquired using a Leica SP8 confocal microscope. Secondary antibodies include: Alexa Fluor™ 488 goat anti-rabbit IgG (H + L), Texas Red® goat anti-rabbit IgG (H + L), Alexa Fluor™ 568 goat anti-mouse IgG (H + L), Alexa Fluor™ 555 donkey anti-goat IgG (H + L) (all Invitrogen).

For haematoxylin and eosin (H&E) staining, slides were thawed and rehydrated in ddH_2O. Sections were subjected to standard H&E (Sigma-Aldrich) staining. Images were acquired using the Nikon Eclipse E 600 microscope with Micron 5 camera.

2.10. Dextran uptake assay

On day 22, 50 μg/mL of 10,000 MW dextran Alexa Fluor 488 (D22910, Thermo Fisher Scientific) was added to the basal medium for 48 h. Organoids were then fixed, cryo-protected, embedded, frozen, sectioned, and imaged, as previously described. Images were acquired using a Leica SP8 confocal microscope.

2.11. Kidney organoid dissociation and single-cell isolation

Organoids used in single-cell RNA sequencing experiments were differentiated from a single well of passage 35 hiPSCs. On day 24, six organoids per support matrix were pooled as part of a single independent experiment and dissociated for scRNA-seq. Organoids were washed with ice-cold DPBS. PeptiGels and Matrigel were first manually removed using blunted p10 pipette tips and a fine spatula. The Olympus SZX10 Wide Zoom Stereomicroscope was used during this process to aid in visualising the samples. Remnant hydrogel in wells was then removed using a cell scraper (Starstedt) and by washing with ice-cold DPBS. Organoids were then dissociated on ice using 500 μL of protease solution (5 mM CaCL2, 10 mg/mL Bacillus Licheniformis protease (Sigma-

Aldrich) and 125 U/mL DNase I (Thermo Fisher Scientific). Plates were agitated by hand for 19 min on ice. Every 2 min (for 15 s) the cell/protease solution was titrated using a p1000 pipette and combination of wide bore p1000 (Satorius) and standard p1000 pipette tips. Following this, cells were passed through 70 μm (Miltenyi Biotec) and 40 μm (Corning) diameter strainers into 2 mL ice cold 5% FBS/DPBS (Gibco). The well and each filter were washed with 1 mL 5% FBS/DPBS. Cells were centrifuged (150 *g*, 5 min, 4 °C) and pellets were re-suspended in 4 mL 2% BSA/PBS (Sigma-Aldrich). Cells were pelleted by centrifugation (150 *g*, 5 min, 4 °C), re-suspended in 500 μL 2% BSA/PBS and passed through a 40 μm Flowmi Cell Strainer (Sigma-Aldrich) into LowBind microcentrifuge tubes (Sarstedt). Cell count and viability were determined using a hemocytometer and Trypan Blue (Sigma-Aldrich) staining. Cells were centrifuged (300 *g*, 3 min, 4 °C) and pellets were resuspended in the appropriate volume of 2% BSA/PBS to achieve 1000 cells/μL per condition. Cell counts and viabilities were determined once more to ensure concentrations were in the range of 1000–2000 cells/μL and that there was high cell viability before proceeding.

2.12. Single-cell library preparation, sequencing and analysis

Cells were processed using the 10x Genomics Chromium platform following the Single-Cell 3′ v3.1 protocol. Briefly, the Chromium Next GEM Chip G was loaded with reverse transcriptase (RT) master mix and single cell solutions to achieve targeted recoveries of 3000–4000 cells, according to the manufacturer's protocol. Within the Chromium Controller, Gel Beads-in-Emulsion (GEMs) were formed containing single cells, RT reagents and a single gel bead composed of barcoded oligonucleotides. Following cell lysis and gel bead dissolution, reverse transcription of cellular mRNA resulted in the incorporation of barcoded oligonucleotides into cDNA which was then amplified by PCR. Enzymatic fragmentation, end repair, A-tailing and A-tailing double sided size selection were employed to generate libraries with index read sequences incorporated, as per manufacturer's instructions. Libraries were quantified by Qubit dsDNA High Sensitivity Kit (Thermo Fisher Scientific) and size profiles examined with the High Sensitivity DNA Assay (Agilent). Libraries were sequenced on the NextSeq 500 (Illumina). Sample reads were demultiplexed with BCL2Fastq and initially processed using Cell Ranger v3.1.0. The resulting data was analysed using Seurat v3.1.5 [39]. Alpha4, Alpha5 and Matrigel samples were merged and processed using the standard scTransform pipeline, with the addition of scDblFinder v1.1.8 [40] for the removal of doublets. The Transwell-maintained kidney organoid datasets (Accession No. E-MTAB-11138) were integrated using Harmony v0.1.0 [41].

2.13. Single-cell RNA sequencing visualisation

Figures presented were generated using Seurat [42] and dittoseq packages [43] with customisations made using ggplot2 [44] and Inkscape [45]. In violin plots throughout, the y-axis displays level of gene expression while the x-axis represents number of cells expressing the gene per condition. The top 50 differentially expressed genes (DEGs) per cluster were used for gene ontology (GO) analysis using ToppFun [46]. To measure differences in the expression of ECM components between conditions the GSEA-MSigDB datasets NABA_CORE_MATRISOME and NABA_ECM_REGULATORS were used [47].

2.14. Total RNA isolation and RT-qPCR

For RNA isolation, organoids were pooled and dissociated as in section 2.11. E.Z.N.A Total RNA Kit I (Omega Bio-Tek) was employed for extraction and purification of RNA following the manufacturer's protocol. Purified RNA was quantified using a NanoDrop 2000 Spectrophotometer (Thermo Fisher Scientific). cDNA was then synthesized using a High Capacity cDNA Reverse Transcription Kit (Applied Biosystems) using a T3000 Thermocycler (Biometra). RT-qPCR (QuantStudio 7 Flex Applied Biosystems, Thermo Fisher Scientific) was employed to quantify gene expression from cDNA (10 ng/well) using either PowerUp SYBR Green Master Mix or TaqMan Gene Expression Master Mix (both Applied Biosystems, Thermo Fisher Scientific). GAPDH was used for data normalisation. The following Taqman assays were used: GAPDH (Hs99999905_m1), PDGFRA (Hs00998018_m1), NPHS2 (Hs00922492_m1) and MAP2 (Hs00258900) (All Applied Biosystems, Thermo Fisher Scientific). The following SYBR primers were used for NPHS1: Forward: AGTGTGGCTAAGGGATTACCC Reverse: TCACCGTGAATGTTCTGTTCC.

2.15. Flow cytometry

Organoids were dissociated as in section 2.11. and incubated with DRAQ5 (Biostatus) at 5 μM for 15 min at room temperature to identify nucleated events and propidium iodide (PI) (Sigma-Aldrich) at 1 μg/ml for 15 min at room temperature to determine viability. Cells were analysed on a BD Accuri C6 Flow Cytometer, calibrated following manufacturer specifications. DRAQ5 was excited with the red laser (635 nm) and the main signal was collected with a 675/25 nm band pass filter. PI was excited with a blue laser and the signal was collected with 585/25 and 670LP filters. C6 files were exported as FCS files and reanalysed with FCSExpress Cytometry v.7 (DeNovo Software), excluding aggregates using the pulse signal of the forward scatter detector in area and high. The gating strategy can be observed in Fig. S6A.

2.16. Statistical analysis

GraphPad Prism 7.0 (GraphPad, San Diego, CA, USA) was used for statistical analyses. To compare multiple groups within an experiment, a one-way ANOVA followed by Tukey's multiple comparisons test was used. A student t-test was performed when comparing two groups. P values in figures are reported as: $^{**}p < 0.01$, $^{***}p < 0.001$, $^{****}p < 0.0001$, *n.s.* = not significant.

3. Results and discussion

3.1. Mechanical profiles of Alpha4 and Alpha5 SAPHs

The structural arrangement of the extracellular microenvironment is known to play an instructive role in the process of branching morphogenesis and renal specification [8,48]. Central to the regulation of early kidney development are fibrillar extracellular matrix (ECM) components, such as collagens and fibronectins, whose hierarchical assembly and transient distribution influence fundamental nephrogenic processes including branching and early tubule formation within the primordium [49]. Given the inherent similarities of the native filamentous ECM architecture to fibrillar hydrogels, we hypothesised that SAPHs constitute an appropriate 3D synthetic environment for renal specification.

Different cell culture and organoid systems have been shown to favour varying mechanical properties. For example, intestinal and mesenchymal stem cells have been shown to preferentially differentiate into intestinal organoids and osteoblasts in soft (1.3 kPa) [5] or stiff (34 kPa) [50] environments, respectively. To investigate kidney organoid differentiation within SAPHs of varying mechanical strengths, two peptide hydrogels were used; Alpha4 (soft) and Alpha5 (stiff). TEM analysis of both SAPHs confirmed an ECM-like hydrogel microstructure containing β-sheet rich nanofibres (Fig. 1A). Notably, nanofibres within hydrogels measured in the range of ~3–4 nm in diameter (Fig. S1B), which is typical of *in vivo* fibrillar ECM components (reviewed in Ref. [51]). To confirm the presence of two mechanically distinct microenvironments for organoid differentiation, the biophysical properties of both hydrogels containing kidney organoids in the presence of culture medium was monitored over a 15-day period, the total duration of organoid encapsulation, using oscillatory rheology. Measurements for both hydrogels were taken on day 0 (1 h) and day 15. During this period,

samples were exposed to basal differentiation medium which was replaced at timepoints that corresponded to medium changes in the kidney organoid differentiation protocol (Fig. 1B). On day 15, kidney organoids were removed immediately prior to measurements. Soft solid-like hydrogel behaviour, typical for these systems, was confirmed by the storage shear moduli (G′) being an order of magnitude larger than the loss shear moduli (G″) at low strain (Fig. S1A). On day 0, the G′ of Alpha4 was 1,050 Pa while that of PeptiGel Alpha5 was significantly higher, at 4,310 Pa, thus confirming PeptiGel Alpha5 is a stiffer hydrogel in comparison to Alpha4. Interestingly, when exposed to basal medium + kidney organoids, the G′ for Alpha4 increased to 7,1393 Pa over the course of 15 days (Fig. 1C) while the G′ for Alpha5 increased to 16,533 Pa (Fig. 1D). The increases in G′ upon exposure to cell culture medium have also been reported in similar hydrogel systems [52] and are due to the action of salt and ions screening the charges on the fibres, which encourages fibre aggregation and results in a stiffening of the hydrogel [53]. Crucially, a substantially higher G′ stiffness for Alpha5 was retained in our culture conditions at both timepoints versus Alpha4. Notably, the bulk G' stiffness of both SAPHs did not change significantly in the presence or absence of kidney organoids after 15 days (Fig. S1C). Mass spectroscopy (MS) semi-quantitative analysis of the constituent peptide in both SAPHs revealed that while exposure to medium at 37 °C with regular changes over 15 days reduced the peptide signal, the presence of differentiating organoids did not have a significant effect (Figs. S2A and S2B). In addition to Alpha4 and Alpha5 ± kidney organoids retaining mechanical integrity over 15 days, swelling experiments demonstrated a low degree of degradation with Alpha5 shrinking, in comparison to Alpha4, to ~80% of the gels weight pre-medium exposure (Fig. S2C). While MS analysis showed a reduction in peptide signal over time, both rheological and swelling measurements demonstrated the bulk properties of the hydrogels were not heavily impacted over 15 days. Both SAPHs displayed higher G′ stiffness in comparison to the reported range of <100 Pa for Matrigel [27]. Shear wave elastography (SWE) imaging has demonstrated cortical stiffness in healthy subjects is in the range of 6.6 kPa–11.44 kPa [54]. The mechanical profiles of the SAPHs utilised in this study spanned and exceeded this range of stiffness between day 0 and day 15 of culture, thus providing two contrasting biophysical microenvironments to study cell fate determination. Importantly, because the charge profiles of both SAPHs are the same at physiological pH, effects on cellular differentiation can be solely ascribed to mechanical differences between the scaffolds. Our SAPH characterisation confirmed that kidney organoids could be matured within structurally similar, yet mechanically distinct microenviron ments.

3.2. SAPHs support hiPSC-derived kidney organoid growth and differentiation

A modified version of the Takasato protocol [6] was employed to generate kidney organoids within SAPHs (Fig. 2A). hiPSCs were first differentiated as a monolayer by supplementing with the WNT signalling activator CHIR99021, resulting in the loss of the pluripotency marker OCT4 and the induction of primitive streak. This was confirmed by the expression of Brachyury (T) by day 3 (Fig. 2B). Differentiating cells underwent an epithelial-mesenchymal transition, losing ECAD and gaining NCAD expression. Supplementation with FGF9 and heparin from day 3 subsequently generated intermediate mesoderm-committed cells, marked by PAX2 and HOXD11, from which all cell types of the mammalian kidney emerge [55]. Cells were then exposed to a 5 μM CHIR99021 pulse to induce nephrogenesis, pelleted by centrifugation and transferred to round bottom ultra-low attachment plates for 48 h. Day 7 was chosen to form 3D aggregates as the necessary cell types were present for kidney organoid generation (Fig. 2B, S3A). These aggregates comprising PAX2 and SIX2 (Fig. S3A), which are both markers and co-expressed in the nephron progenitor population [13], were placed in suspension culture from day 7 to day 9 to facilitate cellular compaction for subsequent encapsulation within matrices (Fig. 2A, S3B, S3C). Without 48 h of suspension culture, the morphology of aggregates during encapsulation was greatly compromised (Fig. S3D). Suspension culture has been previously utilised for kidney micro-organoid differentiation [17]. These micro-organoids were differentiated for 18 days in suspension with fibrosis evident only after day 28. To demonstrate that the suspension culture for 48 h utilised in this study did not induce fibrosis, day 9 pellets and the resulting organoids were shown to be negative for the fibrotic marker αSMA (Fig. S3E). Additionally, aggregates from suspension culture and Transwell inserts were comparable on day 9, with nephron progenitor and mesodermal markers PAX2 and NCAD expressed, and LTL and ECAD nephron structures not yet formed (Fig. S3F). By day 24 of differentiation, organoids within each of the synthetic matrices possessed a dense central cellular region and visible tubular formation at the peripheries of organoids, as observed using bright field microscopy (Fig. 2A).

To ensure an appropriate level of organoid viability within hydrogels by day 24 of differentiation, calcein-AM (live) and ethidium-homodimer-1 (dead) staining were employed as a readout of gross toxicity (Fig. 2C). Viability of organoids within SAPHs was compared to organoids differentiated within the animal-derived ECM, Matrigel. Although there is a shift away from Matrigel and similar basement membrane matrices, such as Geltrex, their use remains an integral part of renal cell culture [56,57], kidney organoid protocols [8,14,58,59] and many other organoid systems [4,60,61]. In total, 18 organoids per support matrix were assessed (6 organoids per condition, three independent experiments). Subsequent quantification revealed that both SAPH conditions generated organoids with a high degree of viability, with slight decreases in cell viability noted with increased matrix stiffness (Matrigel: 92.47%, Alpha4: 88.21%, Alpha5: 84.25%) (Fig. 2C). Cell death within the stiff Alpha5 hydrogel was primarily noted in peripheral regions of organoids at the bio-interface, where TEM micrographs and F-actin immunostaining demonstrated the close association between matrix and cells (Fig. S1D). The diffusion of molecules such as nutrients and growth factors in and out of hydrogels is known to be linked to the nature of interactions between the fibrillar network and the solutes, as well as the porosity of the network. The SAPHs utilised have the same charge profile at pH 7, as well as similar fibrillar morphologies and therefore porosities. The expectation is that diffusion of molecules in and out of these hydrogels will be similar. Due to the low mechanical properties of Matrigel, it is likely that fibre distribution and therefore pore sizes are larger. Importantly, regular medium changes were performed including 24 h post encapsulation. This ensured the differentiating organoids received the necessary nutrients for growth and that all hydrogel systems are exposed to the same conditions. Organoids grown in each condition differentiated into complex, heterogeneous structures, indicating the maturing cells received the appropriate signals through the hydrogels. As ethidium-homodimer-1 staining is observed solely at the periphery of Alpha5, we therefore propose that cell survival in stiffer scaffolds is potentially being perturbed by higher mechanical pressure at these bio-interface regions. Overall, these results confirmed that the properties of both SAPHs were not inherently cytotoxic and that the scaffolds could be used to investigate cell fate trajectories within environments of variable stiffness.

Subsequent immunostaining of organoids confirmed the formation of key cell types associated with the development of the maturing nephron within both Alpha4 and Alpha5 SAPHs (Fig. 2D, S4B). Organoids contained $WT1^{+ve}$ podocytes, leading into LTL^{+ve} proximal tubules and were supported by a $Laminin^{+ve}$ basement membrane. Additionally, LTL^{+ve} proximal tubular cells were noted to be adjacent to $ECAD^{+ve}$ distal tubules. Inner luminal areas of tubular epithelia were $ZO\text{-}1^{+ve}$, marking the epithelial tight junctions of these structures. Nephron structures within the kidney organoids were supported by $MEIS1/2/3^{+ve}$ interstitial cells. H&E staining highlighted a dispersed tubular morphology throughout the SAPH-derived organoids by day 24 (Fig. 2D). Additionally, proximal tubule structures formed within the

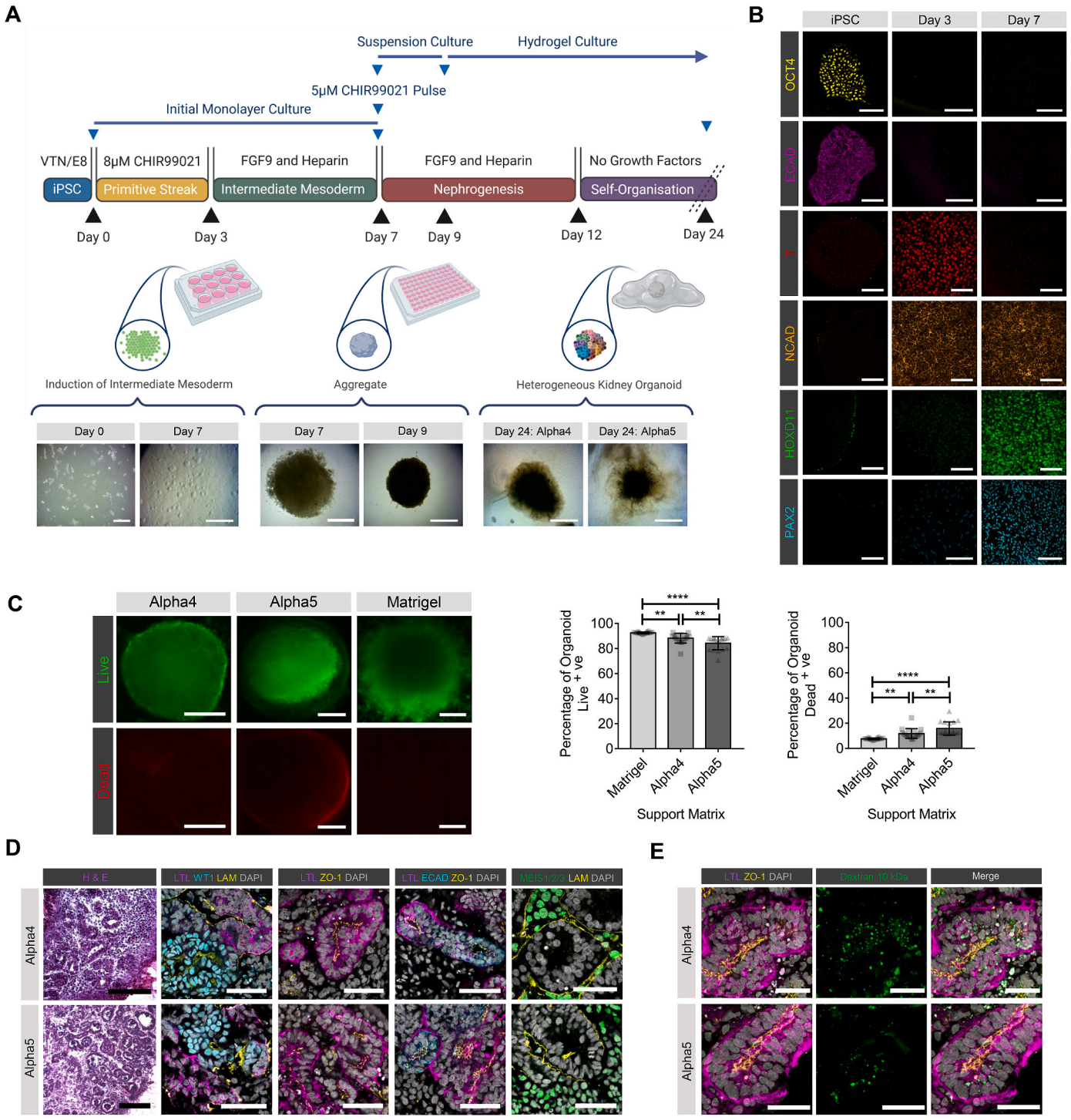

Fig. 2. Differentiation protocol and subsequent characterisation of hiPSC-derived kidney organoids formed within SAPHs. A) hiPSCs were differentiated into kidney progenitors and day 7 aggregates were placed in suspension culture for 48 h. Compacted pellets were encapsulated within Alpha4 or Alpha5 until day 24. Resulting organoids comprised a dense centre with peripheral tubular structures. Day 0 scale bar = 250 μm, rest = 1 mm. **B)** Monolayer immunofluorescent characterisation from pluripotent hiPSCs to day 7 nephron progenitors. Scale bar = 100 μm. **C)** Viability of kidney organoids was compared on day 24 using live (calcein-AM) and dead (ethidium-homodimer-1) stains. Scale bar = 300 μm. Increased matrix stiffness (Matrigel < Alpha4 < Alpha5) had an inverse effect on cell viability. Data expressed as mean ± SD percentage of organoid area positive for live or dead stain with a one-way ANOVA and Tukey's multiple comparisons test used; ** for $p < 0.01$, **** for $p < 0.0001$. N = 18 for each condition from three independent experiments. **D)** H&E and immunofluorescent characterisation of Alpha4 and Alpha5-derived organoids demonstrated successful formation of complex structures and comprised typical cell types of the developing nephron ($WT1^{+ve}$ podocytes, LTL^{+ve} proximal tubules, $ECAD^{+ve}$ distal tubules and $ZO\text{-}1^{+ve}$ epithelial tight junctions) and supporting cells ($MEIS1/2/3^{+ve}$ interstitium and LAM^{+ve} basement membrane). H&E scale bar = 250 μm, immunofluorescence = 50 μm. **E)** Organoids showed functionality by the uptake of fluorescently labelled 10,000 MW dextran. Scale bar = 35 μm.

synthetic hydrogels demonstrated a level of endocytic functionality. LTL^{+ve} proximal tubules, with ZO-1^{+ve} tight junctions marking the lumen, had the capacity to uptake fluorescently labelled dextran (10,000 MW) (Fig. 2E). These results demonstrated a high degree of structural self-organisation within the matrices. Notably, structures generated within SAPHs were shown to be equivalent to those formed on Transwell inserts and within Matrigel (Fig. S4A). We observed that organoids grown in suspension without a matrix or Transwell insert formed renal and supporting cell types. However, these organoids possessed extensive cellular debris and appeared to have reduced structural maturity (Fig. S7A). As a further control, we differentiated organoids on Transwell inserts within Alpha4, Alpha5 and Matrigel. Organoids generated within support matrices ± Transwell inserts similarly formed the same complex structures and supporting cell types

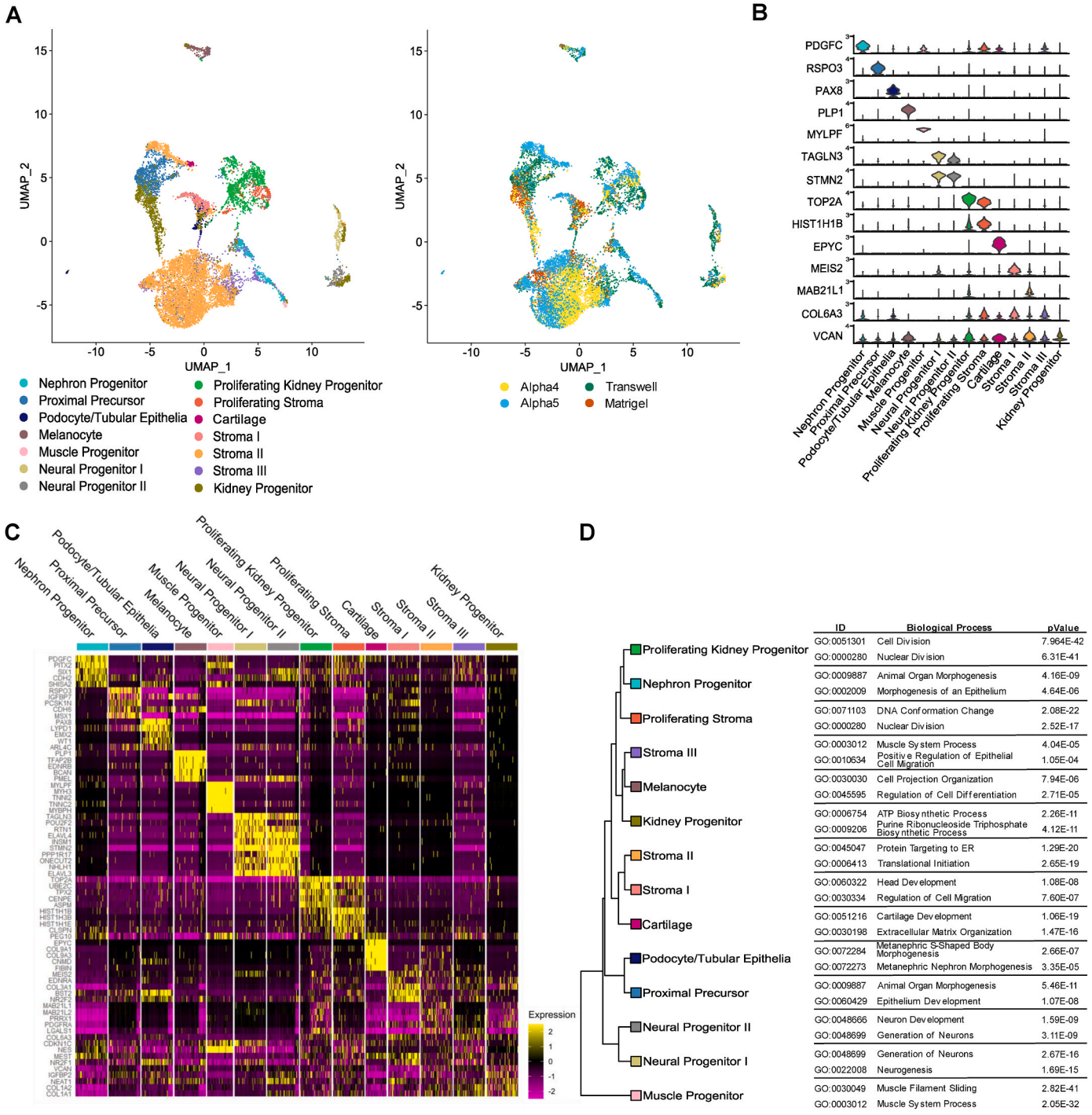

ID	Biological Process	pValue
GO:0051301	Cell Division	7.964E-42
GO:0000280	Nuclear Division	6.31E-41
GO:0009887	Animal Organ Morphogenesis	4.16E-09
GO:0002009	Morphogenesis of an Epithelium	4.64E-06
GO:0071103	DNA Conformation Change	2.08E-22
GO:0000280	Nuclear Division	2.52E-17
GO:0003012	Muscle System Process	4.04E-05
GO:0010634	Positive Regulation of Epithelial Cell Migration	1.05E-04
GO:0030030	Cell Projection Organization	7.94E-06
GO:0045595	Regulation of Cell Differentiation	2.71E-05
GO:0006754	ATP Biosynthetic Process	2.26E-11
GO:0009206	Purine Ribonucleoside Triphosphate Biosynthetic Process	4.12E-11
GO:0045047	Protein Targeting to ER	1.29E-20
GO:0006413	Translational Initiation	2.65E-19
GO:0060322	Head Development	1.08E-08
GO:0030334	Regulation of Cell Migration	7.60E-07
GO:0051216	Cartilage Development	1.06E-19
GO:0030198	Extracellular Matrix Organization	1.47E-16
GO:0072284	Metanephric S-Shaped Body Morphogenesis	2.66E-07
GO:0072273	Metanephric Nephron Morphogenesis	3.35E-05
GO:0009887	Animal Organ Morphogenesis	5.46E-11
GO:0060429	Epithelium Development	1.07E-08
GO:0048666	Neuron Development	1.59E-09
GO:0048699	Generation of Neurons	3.11E-09
GO:0048699	Generation of Neurons	2.67E-16
GO:0022008	Neurogenesis	1.69E-15
GO:0030049	Muscle Filament Sliding	2.82E-41
GO:0003012	Muscle System Process	2.05E-32

Fig. 3. scRNA-seq characterisation of the integrated day 24 kidney organoid dataset. A) The annotated UMAP highlighted fourteen distinct clusters formed in kidney organoids differentiated within Alpha4, Alpha5, Matrigel and on Transwell inserts. The condition from which each cell originated is shown in a separate UMAP and highlights the influence the extracellular environment on cell clustering. **B)** Violin plot of a single differentially expressed gene from each cluster which was used to define the identity of each population. **C)** Heatmap of five differentially expressed genes in each of the fourteen clusters illustrating the unique gene expression pattern in each cluster. **D)** Hierarchical clustering demonstrated similarities and differences between each cluster while gene ontology analysis highlighted biological processes linked with the cell types generated.

(Fig. S4, Fig. S7B).

3.3. scRNA-seq of Alpha4, Alpha5, Transwell and Matrigel integrated dataset highlights diversity of renal cell types within kidney organoids

To further delineate the cell types generated within hydrogels, the transcriptional landscape at the single-cell level was examined. On day 24 of differentiation, single-cell solutions were generated from organoids encapsulated in Alpha4, Alpha5 and Matrigel using mechanical and enzymatic methods. Single-cell transcriptomics was then performed using the 10x Chromium platform. In addition, Harmony [41] was used to perform integrative analysis on Alpha4, Alpha5 and Matrigel-derived organoids with organoids differentiated on Transwell inserts to compare cell types generated in 3D matrices to those grown at an air-liquid interface. Following filtering to remove stressed cells, a total of 13, 179 cells (Alpha4 3,946; Alpha5 3,350; Matrigel 1,764; Transwell 4, 119) were retained for analysis. Cells with greater than 25% mitochondrial reads and with numbers of genes and transcripts further than 2 standard deviations away from the mean were filtered out, in addition to genes expressed in fewer than 5 cells. Unsupervised clustering of the combined integrated dataset was then performed, followed by annotation of the clusters revealing 14 distinct cell types that were visualised using a Uniform Manifold Approximation and Projection (UMAP) (Fig. 3A). The integrated dataset was used so that cell types with similar gene expression profiles in each condition were appropriately clustered together. This subsequently facilitated comparison of cell types within clusters and the identification of clusters with unique gene expression signatures. The cellular identity of each cluster was assigned by comparing differentially expressed genes (DEGs) per cluster to marker genes of known cell types found in literature and by comparing to datasets found in GUDMAP (https://www.gudmap.org/) (Table S1) [62,63]. A violin plot with a representative marker gene from each population is shown (Fig. 3B).

A heat map of the five most significant DEGs per cluster is also shown (Fig. 3C). Clusters identified in the analysis comprised three nephron, four stromal, two kidney progenitor and five non-renal cell types. Of the three nephron-related clusters, the most enriched for progenitor genes was the Nephron Progenitor population. This cluster showed high levels of genes linked with the specification and maintenance of nephron progenitors in renal development including PDGFC [64], SHISA2 [65], EYA1 [66], SIX1 and SIX2 [67] (Fig. 3C, S5A). PITX2 was also differentially expressed in this cluster. This transcription factor has previously been used to increase the induction efficiency of nephron progenitors from human pluripotent stem cells by increasing SIX2 expression [68]. The Proximal Precursor cluster also expressed nephron progenitor genes including RSPO3, which through activation of the canonical WNT pathway [69] regulates this progenitor pool and is essential to their epithelial differentiation [70]. CITED2, whose expression persists in the resulting epithelial structures [71] was also highly expressed in this cluster (Fig. S5A). Importantly, these cells expressed genes found in the developing and differentiated proximal tubule including CDH6, IGFBP7 and PCSK1N. In early stages of kidney development, CDH6 plays a vital role. CDH6 mutations in mice causes decreased nephron number in the adult due to reduced polarisation of the developing tubular epithelia and a failure of nephron fusion to the ureteric bud [72]. CDH6 is expressed in the renal vesicle and its expression persists during early proximal tubule formation [73]. Similarly, IGFBP7 is found in proximal precursors and in adult proximal tubular cells [74] alongside PCSK1N [75]. The third nephron-related cluster, Podocyte/Tubular Epithelia, contained genes largely related to tubular cells of the nephron, but also contained genes expressed by podocytes. DEGs included EMX2 [64], ARL4C [76], KRT18 [77] and ID4 [78] which are found in the varying segments along the developing nephron epithelium. EMX2 [79] and ARL4C [80] are essential genes involved in tubulogenesis, with EMX2 mutant mice lacking a urogenital system. PAX8, a key gene in the specification of nephron segments and branching morphogenesis [81] was similarly highly expressed. A podocyte signature was also present in this cluster, including high expression of WT1 [82] and BST2 [83] which are known markers of human podocytes. WT1, shown to be structurally organised in the kidney organoids (Fig. 2D, S4B), acts as a master regulator of podocyte gene expression, with loss of the gene leading to glomerulosclerosis [84]. Interestingly, a small but distinct population of cells within this cluster expressed genes associated with mature podocytes including NPHS2 (Fig. S5D) [82].

Hierarchical cluster analysis was employed to investigate similarities between the cell types generated (Fig. 3D). The Proximal Precursor and Podocyte/Tubular Epithelia cell types clustered closely together with GO analysis revealing involvement in biological processes such as epithelium development and metanephric nephron morphogenesis, respectively (Fig. 3D). The Nephron Progenitor cells displayed greater similarity to the Proliferating Kidney Progenitor cluster, which, alongside the Proliferating Stroma cluster contained genes relating to cell division including TOP2A and HIST1H1B [85]. The dataset contained three additional clusters of a stromal lineage. Of these, Stroma I and II displayed similarities and thus showed close hierarchical clustering. Stroma I was composed of differentially expressed fetal stromal genes, namely MEIS2 [86], NR2F2 and NR2F1 [87]. The identity of this population was further delineated by the presence of EDNRA and COL3A1, which are highly expressed in each of the stromal populations in the Lindström human fetal kidney dataset [88]. The expression of EDNRA has been shown to play an integral role in the determination of developing renal stromal cell types [89]. Stroma II expressed stromal developmental gene LGALS1 [90], as well as PDGFRA which is linked with renal differentiation processes [91] and is a reported unifying stromal marker in multiple human fetal kidney datasets [64,92]. Additionally, marker genes PRRX1 and MAB21L1 are expressed in stromal progenitor cell types in the fetal kidney [88]. PEG10 and NR2F1 were differentially expressed by Stroma III, with NR2F1 expressed by stromal cells throughout embryonic kidney development in mice [87]. Other marker genes for Stroma III included CDKN1C [93] and COL6A3 [85]. Interestingly, CDKN1C expression in the kidney has been shown to be restricted to a subset of stromal cells in the medulla [94], while COL6A3 expression has previously been shown to be conserved between fetal kidney and organoid datasets [64]. An additional kidney-related cluster was identified from our analysis, Kidney Progenitor, which expressed genes associated with various processes of renal development. For example, VCAN [95] and IGFBP2 [96] which have been reported as nephron progenitor genes. This cluster similarly contained stromal-associated genes such as COL1A1 and COL1A2 [85] and is likely the reason this progenitor population is hierarchically clustered close to Stroma III. However, this population was composed of poor marker genes with DEGs also expressed at high levels in cells outside of the cluster **(Table S1)**. The remaining clusters comprised five prominent off-target non-kidney populations (Fig. 3A). Two neuronal progenitor clusters were identified which shared similar gene expression profiles, including high expression of STMN2 and ELAVL4 [64]. A melanocyte population was present marked by the expression of PLP1 and PMEL [97]. A Muscle Progenitor cluster expressing MYLPF and MYH3 [64] was also identified from the analysis. Additionally, a Cartilage-like cluster was identified comprising genes involved with ECM production and organisation including EPYC, COL9A1 and MATN4 [98]. The single cell transcriptomic data highlighted the diverse populations formed within the organoids, which structurally displayed a high degree of complexity and organisation (Figs. 2D and 4E, S4A, S4B). Structurally, we did not observe spatial differences within organoids, aside from obvious segmentation of epithelial structures (Fig. S4B). Stromal cells were apparent at the periphery of the organoids as evidenced by MEIS1/2/3 expression; however, staining was detected throughout the organoids (Fig. 4E). Recent advances in spatial transcriptomics could be used in the future to stratify gene expression from the periphery to the centre of the organoid to increase our understanding of kidney organoid developmental patterns.

3.4. scRNA-seq reveals cellular heterogeneity within kidney organoids differentiated in varying extracellular growth environments

Once we verified appropriate differentiation of renal cell types within conditions, we next aimed to compare cell populations generated within the two synthetic peptide hydrogels to those formed within Matrigel or on Transwell inserts. Splitting the integrated UMAP by organoid identity and subsequent analysis of the composition of each cluster revealed that the extracellular environment in which the organoids were grown had a significant impact on the cell populations

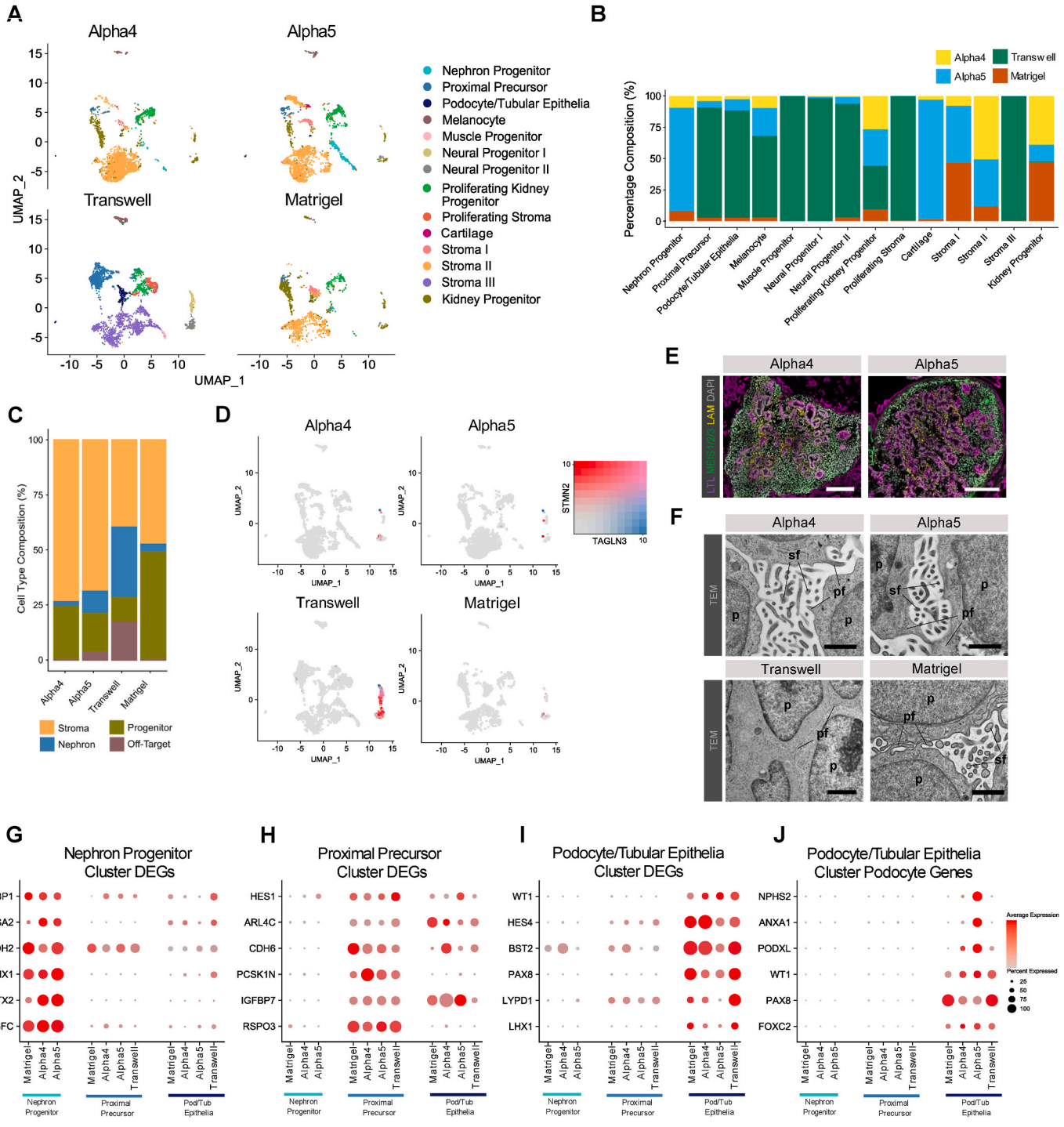

Fig. 4. Day 24 kidney organoid scRNA-seq analysis demonstrates cell type variability when differentiated in varying growth environments. A) UMAP of the integrated dataset was split by the identity of each organoid to highlight the influence of the extracellular environment on the resulting clusters. **B)** The percentage composition of each cluster. **C)** The percentage cell type composition of each condition. **D)** Off-target neuronal cell types were visualised in each organoid by UMAP expression of STMN2 and TAGLN3. **E)** Immunofluorescence of Alpha4 and Alpha5-derived organoids demonstrated an increase level of LTL^{+ve} proximal tubular structures in the stiffer matrix. Scale bar = 200 μm. **F)** TEM micrographs demonstrated the presence of podocyte (p) cell types displaying structures similar to primary foot (pf) processes, with secondary foot (sf) process-like structures present with matrix-derived podocytes. Scale bar = 1 μm **G-I)** Dot plots of the differentially expressed genes from each nephron-related cluster showing average expression and the percentage of cells expressing the genes in each organoid. **J)** Differences in the expression of podocyte signatures within the Podocyte/Tubular Epithelia cluster was examined by dot plot.

generated (Fig. 4A and B). For example, the identity of Stroma I and II were almost completely formed from organoids grown within a three-dimensional environment, whereas Stroma III was almost exclusively associated with Transwell-grown organoids (Fig. 4B). Stroma II and Stroma III clusters comprised a mixture of stromal and kidney progenitor genes which were differentially expressed between the populations (Fig. S5C). Clusters comprising cell types of the same lineage were then grouped and the cell type composition per organoid was examined (Fig. 4C). Organoids which contained the largest proportion of nephron cell types were Transwell-derived, followed by those formed in Alpha5. This is likely due to biophysical differences between encapsulated 3D supports and solid support matrices, such as polyester Transwell inserts.

A small off-target Cartilage-like cluster was identified which was predominantly composed of cells grown within the stiff Alpha5 SAPH. This population contained genes related to the medullary and cortical stromal regions (COL2A1, COL9A3, FIBIN, MGP) [64,99]. However, these cells also had a unique expression pattern associated with cartilage ECM production (COL9A1, EPYC) which is likely due to the stiffer environment (higher G′) within which the organoids were differentiated. This phenomenon was not observed in the low G′ Alpha4 hydrogel or in Matrigel. Given the enrichment of stromal-associated cell populations within SAPH-derived organoids, we compared matrisome and ECM regulator gene expression profiles between conditions using the Naba dataset [47]. The expression of matrisome and ECM regulator genes was highest within Alpha4-derived organoids (Fig. S5B). Additionally, PDGFRA a reported unifying stromal marker [64], whose expression was evident in each stromal population in this dataset (Fig. S6C), was most highly expressed by Alpha4-derived organoids by RT-qPCR (Fig. S6D). These results were consistent with Alpha4 organoids containing the largest proportion of stromal associated cell types (Fig. 4C). This data highlights the importance of assessing matrix production and turnover within encapsulated organoids as the microenvironment is a critical determinant of cell fate.

Transwell organoids did however possess the largest number of off-target cells. These included neural, muscle and melanocyte clusters (Fig. 4B). Examples of highly enriched off-target neuronal genes were visualised by UMAP (Fig. 4D), which highlighted their specificity to Transwell populations. This was also confirmed by RT-qPCR, where Transwell-derived organoids displayed a higher expression of the neuronal marker MAP2 (Fig. S6D). Variable formation of off-target cells is recognised as a significant limitation to current kidney organoid differentiation protocols (reviewed in Refs. [100,101]). Given the reduced off-target signatures within Alpha4, Alpha5 and Matrigel, we propose that the 3D microenvironment offers significant improvements for appropriate cell fate determination. Furthermore, differentiation within synthetic hydrogels reduced the proportion of kidney progenitor cell types observed in the poorly-defined Matrigel growth environment (Fig. 4C). Matrigel-derived organoids contained a much higher percentage of progenitor cell types (up to 50%). A widely accepted limitation of Matrigel is that the poorly-defined biochemical composition adversely impacts cellular differentiation patterns [102,103]. This may also affect the efficiency of differentiation between independent experiments. For example, in this study, TEM analysis of Matrigel-derived organoids possessed podocytes with foot process-like structure. However, in subsequent differentiations various analyses (RT-qPCR, scRNA-seq and immunofluorescent imaging) revealed limited podocyte maturity.

The biophysical environment has previously been reported to elicit control over organoid patterning [5] and influence the generation of specific cell types [104,105]. Both synthetic and natural hydrogels have been utilised to this end, and are emerging as viable alternatives to animal-derived materials. An excellent example is alginate, a natural scaffold, which has been utilised for a range of organoid types [27,106], including the kidney, where it has been used in conjunction with Transwell inserts for 2.5D culture [104]. Similar to SAPHs, alginate provides numerous advantages such as its biocompatibility, ease of handling and low cost. However, as it is a biologically-derived material, variability in its mechanical properties from preparation-to-preparation exists. Synthetic matrices, on the other hand, offer the promise of fully defined conditions while eliminating batch variabilities. Interestingly, this work, in addition to the discussed alginate study [104] demonstrates that the mechanical properties of the microenvironment plays an instructive role over organoid and cellular behaviour without the requirement for adhesion motifs. Our scRNA-seq results further substantiates the role of the 3D bio-interface in refining renal cell types within kidney organoids. Notably, this refinement was achieved using a minimally complex fully synthetic environment.

Further comparison of percentage cell type composition revealed increased nephron formation in Alpha5-derived organoids in comparison to Alpha4 (Fig. 4C). This was reflected by the relative abundance of LTL^{+ve} proximal tubules by immunofluorescence (Fig. 4E). We then compared levels of differentially expressed nephron-associated genes across all conditions. The Nephron Progenitor cluster lacked Transwell-derived cells and was primarily composed of cell types generated within Alpha5. Alpha4 and Alpha5 showed increased expression of PITX2 and SHISA2 over Matrigel organoids (Fig. 4G). These genes have regulatory roles in the induction and self-renewal of nephron progenitor cells [65,68]. The Proximal Precursor cluster displayed similar gene expression profiles among conditions, with selective genes persisting into the Podocyte/Tubular Epithelia cluster (Fig. 4H). Transwell-derived cells comprised the majority of the Podocyte/Tubular Epithelia cluster and showed an enrichment of nephron specifying genes LHX1 and LYPD1 (Fig. 4I) [88,107]. Each condition showed similar expression of immature podocyte markers FOXC2, PAX8 and WT1 (Fig. 4J), however, Alpha5-derived organoids showed increased expression of mature podocyte genes including NPHS2, ANXA1 and PODXL. This trend was reflected by RT-qPCR where Alpha5-derived organoids displayed higher expression of NPHS2 and NPHS1 (Fig. S6D). While stiffer microenvironments have previously been shown to favour podocyte differentiation [108], Alpha4 organoids did show some expression of mature podocyte genes (PODXL). Notably, TEM micrographs of Transwell-derived organoids lacked structural components associated with mature podocytes. In contrast, organoids differentiated within a support matrix were shown to possess podocytes with more mature structural features, including primary and secondary foot process-like structures (Fig. 4F).

As technologies to investigate the transcriptome have developed in recent years, it is becoming increasingly apparent that different approaches have distinct advantages and disadvantages. For example, scRNA-seq allows for the characterisation of heterogeneous organs such as the kidney and the identification of rare cell populations. However, single cell transcriptomic data is inherently noisy and requires more complex bioinformatic tools compared to bulk RNA-seq. The adaptation of a set of guidelines or standards for analyses and quality control is an urgent need. This study has been guided by best current practice including the pooling of cells from multiple organoids. Additionally, the cold active protease *Bacillus Licheniformis* was employed to minimize gene expression alterations and the generation of gene expression artifacts during dissociation [109]. During method development, we widely employed flow cytometry to quantify our population and ensure dispersal. Results indicated that after dissociation, cells were 91%–98% viable, confirming no appreciable cell loss (Fig. S6A).

However, limitations still exist particularly in the initial dissociation where it has been reported that epithelial cells may be depleted [64]. Care must also be taken during comparative studies as sample-to-sample, and cell line-to-cell line variation is common and must be controlled for. For example, previous reports using Transwell-derived organoids have demonstrated derivation of podocytes with a more mature signature [6]. However in this study, this level of maturation was lacking in Transwell-derived organoids as confirmed by scRNA-seq, RT-qPCR, TEM and fluorescent imaging suggesting a level of variability between iPSC lines which, while somewhat limiting, is not

surprising considering their different origin and degree of pluripotency. Importantly, RT-qPCR reflected gene expression trends observed by scRNA-seq such as the increased level of stromal marker PDGFRA and reduced expression of the neuronal marker MAP2 in encapsulated organoids. Improved maturity of podocytes in the stiff Alpha5 hydrogel was also identified (Fig. S6D). To further validate that these results are due to the presence of an ECM, a similar trend was found when organoids were cultured within each of the respective matrices, grown on Transwell inserts (Fig. S7C). Interestingly, PDGFRA expression in organoids grown within matrices on Transwell inserts was reduced when compared to the original culture method (Figs. S6D and S7C). This supports the idea that Transwell culture may reduce stromal formation.

Stiffness has been shown to have regional-specific effects on developing organoids [110]. It is likely that different cell types within an organ favour varying stiffness profiles, as was the case with podocytes in this study. Due to this, developments in peptide hydrogel bioprinting technologies [111,112] could be employed in the future to generate stiffness gradients and enable cell-type specific maturation and concurrently improve our understanding of ECM mechanics within organs. Such advances could also be used to investigate the emergence of the various cell types of the kidney over extended culture periods within varying stiffness gradients. Maturation of the nephron may be dependent both on culture time and mechanical influence. Developmentally, podocytes have been shown to emerge first from the nephron progenitor pool [113]. Therefore, extended culture could result in enhanced maturation of residual proximal and distal cells within hydrogels. Additionally, technologies such as spatial transcriptomics could reveal the cellular location of mature gene signatures in response to these mechanical influences.

Much of the impetus in the kidney regenerative therapeutics field is being driven by the overarching aims of the '(Re)Building a Kidney' consortium [114]. The first iterations of stem cell-derived kidney organoids were lacking in maturity, vascularity and had no appropriate input or output mechanism. Since then, significant efforts to aid maturation have been undertaken. Further translation towards human studies requires support matrices that are not only biocompatible, but are approved for use in humans. In this regard, SAPHs have many favourable characteristics, notably the ability to define biomechanical properties in a fully-synthetic matrix that facilitates the differentiation of specific cell types. The successful example of bringing stem cell-derived pancreatic progenitor cells to clinical trial for the treatment of Type I Diabetes ([115], NCT02239354) provides an excellent template for how the transplantation of stem cell-derived nephrons will benefit patients with Chronic Kidney Disease (CKD) in the era of Next-Generation Therapeutics.

4. Conclusion

The translational utility of kidney organoids relies on the ability to grow tissues within physiologically relevant and non-xenogenic microenvironments that enable the controlled differentiation of renal cell types. We highlight self-assembling peptide hydrogels (SAPHs) as a 3D biomimetic environment for the specification of hiPSC-derived kidney organoids. The functional renal cell types generated within SAPHs demonstrates that minimally complex synthetic matrices are sufficient for kidney organoid culture, thus negating the requirement for complex, poorly defined animal-derived matrices such as Matrigel. Using scRNA-seq, we also reveal the influence of the *in vitro* growth environment in generating compositionally distinct cell types and perturbing cell fate determination. The stiffer matrix, Alpha5, generated organoids with an increased proportion of nephron cell types containing more mature podocyte signatures in comparison to the softer matrix, Alpha4. Compared to kidney organoids grown at the air-liquid interface, organoids generated within 3D matrices possessed reduced off-target cell types, illustrating the influence of the biophysical environment for appropriate cell fate specification. To the best of our knowledge, this is the first investigation of hiPSC-derived kidney organoids embedded within fully synthetic peptide-based hydrogels. These results will further support the global effort to produce viable replacement organs from hiPSCs.

Funding sources

This publication has emanated from research conducted with the financial support of Science Foundation Ireland (SFI) and is co-funded under the European Regional Development Fund under Grant Number 13/RC/2073_P2. The authors acknowledge support from Science Foundation Ireland (16/IA/4584) and 19/FFP/6833. J.K.W. would also like to acknowledge Royal Society of Chemistry grant (M19-6613).

Author Contributions

N.J.T. and S.C. carried out the experimental work and wrote the manuscript. J.L.D. and J.K.W. also performed experimental work. C.K. performed scRNA-seq analysis. J.C. designed the study and edited the manuscript with assistance from D.F.B., J.K.W., A.F.M. and A.S.

Notes

Co-first authors can prioritise their names when adding this paper's reference to their resumes. This work was supported, in part, by contribution from Manchester BIOGEL. All research data supporting this publication are directly available within this publication and associated supporting information. Single cell data is available at https://www.ebi.ac.uk/arrayexpress/, accession number, E-MTAB-11149.

Declaration of interest statement

This work was supported, in part, by contribution from Manchester BIOGEL.

Ethics approval and consent to participate

The manuscript is not related to a clinical study, nor does it involve experimentation on animals nor involve human subjects.

Acknowledgements

Certain components of figures were generated using BioRender.com. The authors thank Tiina O'Neill of the Conway Institute of Biomolecular and Biomedical Research Imaging Core for her expertise in TEM. Confocal microscopy was carried out at the Nano Research Facility, Dublin City University which was funded under the Programme for Research in Third Level Institutions (PRTLI) Cycle 5. The PRTLI is co-funded through the European Regional Development Fund (ERDF), part of the European Union Structural Funds Programme 2011–2015. The authors thank Dr Jimmy Muldoon of the UCD School of Chemistry for his expertise in mass spectroscopy. MS-based research reported in this publication was supported by The Comprehensive Molecular Analysis Platform (CMAP) under The SFI Research Infrastructure Programme, reference 18/RI/5702, and BiOrbic, the SFI Bioeconomy Research Centre, and with the support of the School of Chemistry and UCD. The authors thank Dr Alfonso Blanco, director of the Conway Institute of Biomolecular and Biomedical Research Flow Cytometry Core Technologies for his expertise.

Appendix A. Supplementary data

Supplementary data to this article can be found online at https://doi.org/10.1016/j.bioactmat.2022.08.003.

References

[1] J.A. Thomson, J. Itskovitz-Eldor, S.S. Shapiro, M.A. Waknitz, J.J. Swiergiel, V. S. Marshall, J.M. Jones, Embryonic stem cell lines derived from human blastocysts, Science 282 (5391) (1998) 1145–1147, https://doi.org/10.1126/science.282.5391.1145.

[2] K. Takahashi, K. Tanabe, M. Ohnuki, M. Narita, T. Ichisaka, K. Tomoda, S. Yamanaka, Induction of pluripotent stem cells from adult human fibroblasts by defined factors, Cell 131 (5) (2007) 861–872, https://doi.org/10.1016/j.cell.2007.11.019.

[3] P. Hoang, J. Wang, B.R. Conklin, K.E. Healy, Z. Ma, Generation of spatial-patterned early-developing cardiac organoids using human pluripotent stem cells, Nat. Protoc. 13 (2018) 723–737, https://doi.org/10.1038/nprot.2018.006.

[4] M.A. Lancaster, J.A. Knoblich, Generation of cerebral organoids from human pluripotent stem cells, Nat. Protoc. 9 (2014) 2329–2340, https://doi.org/10.1038/nprot.2014.158.

[5] N. Gjorevski, N. Sachs, A. Manfrin, S. Giger, M.E. Bragina, P. Ordóñez-Morán, H. Clevers, M.P. Lutolf, Designer matrices for intestinal stem cell and organoid culture, Nature 539 (2016) 560–564, https://doi.org/10.1038/nature20168.

[6] M. Takasato, P.X. Er, H.S. Chiu, B. Maier, G.J. Baillie, C. Ferguson, R.G. Parton, E. J. Wolvetang, M.S. Roost, S.M. Chuva de Sousa Lopes, M.H. Little, Kidney organoids from human iPS cells contain multiple lineages and model human nephrogenesis, Nature 526 (7574) (2015) 564–568, https://doi.org/10.1038/nature15695.

[7] X. Zhong, C. Gutierrez, T. Xue, C. Hampton, M.N. Vergara, L.H. Cao, A. Peters, T. S. Park, E.T. Zambidis, J.S. Meyer, D.M. Gamm, K.W. Yau, M.V. Canto-Soler, Generation of three-dimensional retinal tissue with functional photoreceptors from human iPSCs, Nat. Commun. 5 (2014) 4047, https://doi.org/10.1038/ncomms5047.

[8] N. Cruz, X. Song, S. Czerniecki, R.E. Gulieva, A.J. Churchill, Y.K. Kim, K. Winston, L.M. Tran, M.A. Diaz, H. Fu, L.S. Finn, Y. Pei, J. Himmelfarb, B.S. Freedman, Organoid cystogenesis reveals a critical role of microenvironment in human polycystic kidney disease, Nat. Mater. 16 (2017) 1112–1119, https://doi.org/10.1038/nmat4994.

[9] L. Huang, A. Holtzinger, I. Jagan, M. BeGora, I. Lohse, N. Ngai, C. Nostro, R. Wang, L.B. Muthuswamy, H.C. Crawford, C. Arrowsmith, S.E. Kalloger, D. J. Renouf, A.A. Connor, S. Cleary, D.F. Schaeffer, M. Roehrl, M.S. Tsao, S. Gallinger, G. Keller, S.K. Muthuswamy, Ductal pancreatic cancer modeling and drug screening using human pluripotent stem cell– and patient-derived tumor organoids, Nat. Med. 21 (2015) 1364–1371, https://doi.org/10.1038/nm.3973.

[10] N. Phan, J.J. Hong, B. Tofig, M. Mapua, D. Elashoff, N.A. Moatamed, J. Huang, S. Memarzadeh, R. Damoiseaux, A. Soragni, A simple high-throughput approach identifies actionable drug sensitivities in patient-derived tumor organoids, Commun. Biol. 2 (2019) 78, https://doi.org/10.1038/s42003-019-0305-x.

[11] Y. Saito, T. Muramatsu, Y. Kanai, H. Ojima, A. Sukeda, N. Hiraoka, E. Arai, Y. Sugiyama, J. Matsuzaki, R. Uchida, N. Yoshikawa, R. Furukawa, H. Saito, Establishment of patient-derived organoids and drug screening for biliary tract carcinoma, Cell Rep. 27 (4) (2019) 1265–1276, https://doi.org/10.1016/j.celrep.2019.03.088.

[12] C. Boreström, A. Jonebring, J. Guo, H. Palmgren, L. Cederblad, A. Forslöw, A. Svensson, M. Söderberg, A. Reznichenko, J. Nyström, J. Patrakka, R. Hicks, M. Maresca, B. Valastro, A. Collén, A CRISP(e)R view on kidney organoids allows generation of an induced pluripotent stem cell–derived kidney model for drug discovery, Kidney Int. 94 (6) (2018) 1099–1110, https://doi.org/10.1016/j.kint.2018.05.003.

[13] R. Morizane, A.Q. Lam, B.S. Freedman, S. Kishi, M.T. Valerius, J.V. Bonventre, Nephron organoids derived from human pluripotent stem cells model kidney development and injury, Nat. Biotechnol. 33 (11) (2015) 1193–1200, https://doi.org/10.1038/nbt.3392.

[14] B.S. Freedman, C.R. Brooks, A.Q. Lam, H. Fu, R. Morizane, V. Agrawal, A.F. Saad, M.K. Li, M.R. Hughes, R.V. Werff, D.T. Peters, J. Lu, A. Baccei, A.M. Siedlecki, M. T. Valerius, K. Musunuru, K.M. McNagny, T.I. Steinman, J. Zhou, P.H. Lerou, J. V. Bonventre, Modelling kidney disease with CRISPR-mutant kidney organoids derived from human pluripotent epiblast spheroids, Nat. Commun. 6 (2015) 8715, https://doi.org/10.1038/ncomms9715.

[15] A. Taguchi, R. Nishinakamura, Higher-order kidney organogenesis from pluripotent stem cells, Cell Stem Cell 21 (6) (2017) 730–746, https://doi.org/10.1016/j.stem.2017.10.011.

[16] A. Przepiorski, V. Sander, T. Tran, J.A. Hollywood, B. Sorrenson, J.H. Shih, E. J. Wolvetang, A.P. McMahon, T.M. Holm, A.J. Davidson, A simple bioreactor-based method to generate kidney organoids from pluripotent stem cells, Stem Cell Rep. 11 (2) (2018) 470–484, https://doi.org/10.1016/j.stemcr.2018.06.018.

[17] S.V. Kumar, P.X. Er, K.T. Lawlor, A. Motazedian, M. Scurr, I. Ghobrial, A. N. Combes, L. Zappia, A. Oshlack, E.G. Stanley, M.H. Little, Kidney micro-organoids in suspension culture as a scalable source of human pluripotent stem cell-derived kidney cells, Development 146 (2019) 5, https://doi.org/10.1242/dev.172361.

[18] K.A. Homan, N. Gupta, K.T. Kroll, D.B. Kolesky, M. Skylar-Scott, T. Miyoshi, D. Mau, M.T. Valerius, T. Ferrante, J.V. Bonventre, J.A. Lewis, R. Morizane, Flow-enhanced vascularization and maturation of kidney organoids in vitro, Nat. Methods 16 (3) (2019) 255–262, https://doi.org/10.1038/s41592-019-0325-y.

[19] K.H. Vining, D.J. Mooney, Mechanical forces direct stem cell behaviour in development and regeneration, Nat. Rev. Mol. Cell Biol. 18 (12) (2017) 728–742, https://doi.org/10.1038/nrm.2017.108.

[20] J.M. Muncie, V.M. Weaver, The physical and biochemical properties of the extracellular matrix regulate cell fate, Curr. Top. Dev. Biol. 130 (2018) 1–37, https://doi.org/10.1016/bs.ctdb.2018.02.002.

[21] C.F. Guimarães, L. Gasperini, A.P. Marques, R.L. Reis, The stiffness of living tissues and its implications for tissue engineering, Nat. Rev. Mater. (2020), https://doi.org/10.1038/s41578-019-0169-1.

[22] M. Cantini, H. Donnelly, M.J. Dalby, M. Salmeron-Sanchez, The plot thickens: the emerging role of matrix viscosity in cell mechanotransduction, Adv. Healthcare Mater. 9 (2020), 1901259, https://doi.org/10.1002/adhm.201901259.

[23] B.A. Lindborg, J.H. Brekke, A.L. Vegoe, C.B. Ulrich, K.T. Haider, S. Subramaniam, S.L. Venhuizen, C.R. Eide, P.J. Orchard, W. Chen, Q. Wang, F. Pelaez, C.M. Scott, E. Kokkoli, S.A. Keirstead, J.R. Dutton, J. Tolar, T.D. O'Brien, Rapid induction of cerebral organoids from human induced pluripotent stem cells using a chemically defined hydrogel and defined cell culture medium, Stem Cells Translational Medicine 5 (7) (2016) 970–979, https://doi.org/10.5966/sctm.2015-0305.

[24] R. Cruz-Acuña, M. Quirós, S. Huang, D. Siuda, J.R. Spence, A. Nusrat, A.J. García, PEG-4MAL hydrogels for human organoid generation, culture, and in vivo delivery, Nat. Protoc. 13 (2018) 2102–2119, https://doi.org/10.1038/s41596-018-0036-3.

[25] P. Zhang, L. Xu, J. Gao, G. Xu, Y. Song, G. Li, J. Ren, Y. Zhang, C. Yang, Y. Zhang, R. Xie, N. Zhang, H. Yang, 3D collagen matrices modulate the transcriptional trajectory of bone marrow hematopoietic progenitors into macrophage lineage commitment, Bioact. Mater. 10 (2022) 255–268, https://doi.org/10.1016/j.bioactmat.2021.08.032.

[26] C.-C. Hsu, J.H. George, S. Waller, C. Besnard, D.A. Nagel, E.J. Hill, M.D. Coleman, A.M. Korsunsky, A. Cui, H. Ye, Increased connectivity of hiPSC-derived neural networks in multiphase granular hydrogel scaffolds, Bioact. Mater. 9 (2022) 358–372, https://doi.org/10.1016/j.bioactmat.2021.07.008.

[27] M.M. Capeling, M. Czerwinski, S. Huang, Y.-H. Tsai, A. Wu, M.S. Nagy, B. Juliar, N. Sundaram, Y. Song, W.M. Han, S. Takayama, E. Alsberg, A.J. Garcia, M. Helmrath, A.J. Putnam, J.R. Spence, Nonadhesive alginate hydrogels support growth of pluripotent stem cell-derived intestinal organoids, Stem Cell Rep. 12 (2019) 381–394, https://doi.org/10.1016/j.stemcr.2018.12.001.

[28] X. Ma, A. Agas, Z. Siddiqui, K. Kim, P. Iglesias-Montoro, J. Kalluru, V. Kumar, J. Haorah, Angiogenic peptide hydrogels for treatment of traumatic brain injury, Bioact. Mater. 5 (1) (2020) 124–132, https://doi.org/10.1016/j.bioactmat.2020.01.005.

[29] D. Kumar, V.L. Workman, M. O'Brien, J. McLaren, L. White, K. Ragunath, F. Rose, A. Saiani, J.E. Gough, Peptide hydrogels—a tissue engineering strategy for the prevention of oesophageal strictures, Adv. Funct. Mater. 27 (2017), 1702424, https://doi.org/10.1002/adfm.201702424.

[30] S. Zhang, T. Holmes, C. Lockshin, A. Rich, Spontaneous assembly of a self-complementary oligopeptide to form a stable macroscopic membrane, Proc. Natl. Acad. Sci. USA 90 (8) (1993) 3334–3338, https://doi.org/10.1073/pnas.90.8.3334.

[31] J.K. Wychowaniec, A.M. Smith, C. Ligorio, O.O. Mykhaylyk, A.F. Miller, A. Saiani, Role of sheet-edge interactions in β-sheet self-assembling peptide hydrogels, Biomacromolecules 21 (6) (2020) 2285–2297, https://doi.org/10.1021/acs.biomac.0c00229.

[32] D. VAN Slyke, Physiology of the amino acids, Nature 149 (1942) 342–345, https://doi.org/10.1038/149342a0.

[33] J. Gao, C. Tang, M.A. Elsawy, A.M. Smith, A.F. Miller, A. Saiani, Controlling self-assembling peptide hydrogel properties through network topology, Biomacromolecules 18 (3) (2017) 826–834, https://doi.org/10.1021/acs.biomac.6b01693.

[34] S. Wan, S. Borland, S.M. Richardson, C.L.R. Merry, A. Saiani, J.E. Gough, Self-assembling peptide hydrogel for intervertebral disc tissue engineering, Acta Biomater. 46 (2016) 29–40, https://doi.org/10.1016/j.actbio.2016.09.033.

[35] Y. Qi, H. Min, A. Mujeeb, Y. Zhang, X. Han, X. Zhao, G.J. Anderson, Y. Zhao, G. Nie, Injectable hexapeptide hydrogel for localized chemotherapy prevents breast cancer recurrence, ACS Appl. Mater. Interfaces 10 (8) (2018) 6972–6981, https://doi.org/10.1021/acsami.7b19258.

[36] Y. Kobayashi, J. Nouet, E. Baljinnyam, Z. Siddiqui, D.H. Fine, D. Fraidenraich, V. A. Kumar, E. Shimizu, iPSC-derived cranial neural crest-like cells can replicate dental pulp tissue with the aid of angiogenic hydrogel, Bioact. Mater. (2021), https://doi.org/10.1016/j.bioactmat.2021.11.014.

[37] J. Schindelin, I. Arganda-Carreras, E. Frise, V. Kaynig, M. Longair, T. Pietzsch, S. Preibisch, C. Rueden, S. Saalfeld, B. Schmid, J.Y. Tinevez, D.J. White, V. Hartenstein, K. Eliceiri, P. Tomancak, A. Cardona, Fiji: an open-source platform for biological-image analysis, Nat. Methods 9 (7) (2012) 676–682, https://doi.org/10.1038/nmeth.2019.

[38] J.F. Dekkers, M. Alieva, L.M. Wellens, H.C.R. Ariese, P.R. Jamieson, A.M. Vonk, G.D. Amatngalim, H. Hu, K.C. Oost, H.J.G. Snippert, J.M. Beekman, E.J. Wehrens, J.E. Visvader, H. Clevers, A.C. Rios, High-resolution 3D imaging of fixed and cleared organoids, Nat. Protoc. 14 (2019) 1756–1771, https://doi.org/10.1038/s41596-019-0160-8.

[39] T. Stuart, A. Butler, P. Hoffman, C. Hafemeister, E. Papalexi, W.M. M III, Y. Hao, M. Stoeckius, P. Smibert, R. Satija, Comprehensive integration of single-cell data, Cell 177 (2019) 1888–1902, https://doi.org/10.1016/j.cell.2019.05.031.

[40] P. Germain, scDblFinder: scDblFinder. R package version 1.1.8. https://github.com/plger/scDblFinder, 2020.

[41] I. Korsunsky, J. Fan, K. Slowikowski, F. Zhang, K. Wei, Y. Baglaenko, M. Brenner, P.-R. Loh, S. Raychaudhuri, Fast, sensitive, and accurate integration of single cell data with Harmony, Nat. Methods 16 (2019) 1289–1296, https://doi.org/10.1038/s41592-019-0619-0.

[42] Y. Hao, S. Hao, E. Andersen-Nissen, W.M. M III, S. Zheng, A. Butler, M.J. Lee, A. J. Wilk, C. Darby, M. Zagar, P. Hoffman, M. Stoeckius, E. Papalexi, E.P. Mimitou, J. Jain, A. Srivastava, T. Stuart, L.B. Fleming, B. Yeung, A.J. Rogers, J. M. McElrath, C.A. Blish, R. Gottardo, P. Smibert, R. Satija, Integrated analysis of multimodal single-cell data, Cell 184 (13) (2021) 3573–3587, https://doi.org/10.1016/j.cell.2021.04.048, e29.
[43] D.G. Bunis, J. Andrews, G.K. Fragiadakis, T.D. Burt, M. Sirota dittoSeq, Universal user-friendly single-cell and bulk RNA sequencing visualization toolkit, Bioinformatics 36 (22–23) (2020) 5535–5536, https://doi.org/10.1093/bioinformatics/btaa1011.
[44] H. Wickham, ggplot2: Elegant Graphics for Data Analysis, 2 ed., Springer International Publishing, New York, 2016, p. 260.
[45] Inkscape Contributors. Inkscape, V1.0.1, inkscape.Org.
[46] J. Chen, E.E. Bardes, B.J. Aronow, A.G. Jegga, ToppGene Suite for gene list enrichment analysis and candidate gene prioritization, Nucleic Acids Res. 37 (2009) W305–W311, https://doi.org/10.1093/nar/gkp42.
[47] A. Naba, K.R. Clauser, S. Hoersch, H. Liu, S.A. Carr, R.O. Hynes, The matrisome: in silico definition and in vivo characterization by proteomics of normal and tumor extracellular matrices, Mol. Cell. Proteomics 11 (4) (2012), 014647, https://doi.org/10.1074/mcp.M111.014647–1. M111.
[48] C.M. Nelson, M.M. Vanduijn, J.L. Inman, D.A. Fletcher, M.J. Bissell, Tissue geometry determines sites of mammary branching morphogenesis in organotypic cultures, Science 13 (5797) (2006) 298–300, https://doi.org/10.1126/science.1131000, 314.
[49] P. Ye, S.L. Habib, J.M. Ricono, N. Kim, G.G. Choudhury, J.L. Barnes, H.E. Abboud, M.Y. Arar, Fibronectin induces ureteric bud cells branching and cellular cord and tubule formation, Kidney Int. 66 (4) (2004) 1356–1364, https://doi.org/10.1111/j.1523-1755.2004.00897.x.
[50] A.J. Engler, S. Sen, H.L. Sweeney, D.E. Discher, Matrix elasticity directs stem cell lineage specification, Cell 25 (4) (2006) 677–689, https://doi.org/10.1016/j.cell.2006.06.044, 126.
[51] E. Prince, E. Kumacheva, Design and applications of man-made biomimetic fibrillar hydrogels, Nat. Rev. Mater. 4 (2019) 99–115, https://doi.org/10.1038/s41578-018-0077-9.
[52] C. Ligorio, M. Zhou, J.K. Wychowaniec, X. Zhu, C. Bartlam, A.F. Miller, A. Vijayaraghavan, J. Hoyland, A. Saiani, Graphene oxide containing self-assembling peptide hybrid hydrogels as a potential 3D injectable cell delivery platform for intervertebral disc repair applications, Acta Biomater. 92 (2019) 92–103, https://doi.org/10.1016/j.actbio.2019.05.004.
[53] F. Koch, M. Müller, F. König, N. Meyer, J. Gattlen, U. Pieles, K. Peters, B. Kreikemeyer, S. Mathes, S. Saxer, Mechanical characteristics of beta sheet-forming peptide hydrogels are dependent on peptide sequence, concentration and buffer composition, R. Soc. Open Sci. 5 (3) (2018), https://doi.org/10.1098/rsos.171562.
[54] K. Hassan, N. Loberant, N. Abbas, H. Fadi, H. Shadia, K. Khazim, Shear wave elastography imaging for assessing the chronic pathologic changes in advanced diabetic kidney disease, Therapeut. Clin. Risk Manag. 7 (12) (2016) 1615–1622, https://doi.org/10.2147/TCRM.S118465.
[55] L. Saxén, H. Sariola, Early organogenesis of the kidney, Pediatr. Nephrol. 1 (1987) 385–392, https://doi.org/10.1007/BF00849241.
[56] H. Beaton, D. Andrews, M. Parsons, M. Murphy, A. Gaffney, D. Kavanagh, G. J. McKay, A.P. Maxwell, C.T. Taylor, E.P. Cummins, C. Godson, D.F. Higgins, P. Murphy, J. Crean, Wnt6 regulates epithelial cell differentiation and is dysregulated in renal fibrosis, Am. J. Physiol. Ren. Physiol. 1 (1) (2016) F35–F45, https://doi.org/10.1152/ajprenal.00136.2016, 311.
[57] T.C. Chen, M. Neupane, S.J. Chien, F.R. Chuang, R.B. Crawford, N.E. Kaminski, C. C. Chang, Characterization of adult canine kidney epithelial stem cells that give rise to dome-forming tubular cells, Stem Cell. Dev. 1 (21) (2019) 1424–1433, https://doi.org/10.1089/scd.2019.0049, 28.
[58] Z. Zeng, B. Huang, R.K. Parvez, Y. Li, J. Chen, A.C. Vonk, M.E. Thornton, T. Patel, E.A. Rutledge, A.D. Kim, J. Yu, B.H. Grubbs, J.A. McMahon, N.M. Pastor-Soler, K. R. Hallows, A.P. McMahon, Z. Li, Generation of patterned kidney organoids that recapitulate the adult kidney collecting duct system from expandable ureteric bud progenitors, Nat. Commun. 12 (2021) 3641, https://doi.org/10.1038/s41467-021-23911-5.
[59] D-y. Jun, S.Y. Kim, J.C. Na, H.H. Lee, J. Kim, Y.E. Yoon, S.J. Hong, W.K. Han, Tubular organotypic culture model of human kidney, PLoS One 13 (10) (2018), e0206447, https://doi.org/10.1371/journal.pone.0206447.
[60] A.J. Miller, B.R. Dye, D. Ferrer Torres, D.R. Hill, A.W. Overeem, L.D. Shea, J. R. Spence, Generation of lung organoids from human pluripotent stem cells in vitro, Nat. Protoc. 14 (2019) 518–540, https://doi.org/10.1038/s41596-018-0104-8.
[61] S.E. Hocevar, L. Liu, R.K. Duncan, Matrigel is required for efficient differentiation of isolated, stem cell-derived otic vesicles into inner ear organoids, Stem Cell Res. 53 (2021), 102295, https://doi.org/10.1016/j.scr.2021.102295.
[62] S.D. Harding, C. Armit, J. Armstrong, J. Brennan, Y. Cheng, B. Haggarty, D. Houghton, S. Lloyd-MacGilp, X. Pi, Y. Roochun, M. Sharghi, C. Tindal, A. P. McMahon, B. Gottesman, M.H. Little, K. Georgas, B.J. Aronow, S.S. Potter, E. W. Brunskill, E.M. Southard-Smith, C. Mendelsohn, R.A. Baldock, J.A. Davies, D. Davidson, The GUDMAP database–an online resource for genitourinary research, Development 138 (2011) 2845–2853, https://doi.org/10.1242/dev.063594.
[63] A.P. McMahon, B.J. Aronow, D.R. Davidson, J.A. Davies, K.W. Gaido, S. Grimmond, J.L. Lessard, M.H. Little, S.S. Potter, E.L. Wilder, P. Zhang, GUDMAP: the genitourinary developmental molecular anatomy project, J. Am. Soc. Nephrol. 19 (2008) 667–671, https://doi.org/10.1681/ASN.2007101078.
[64] A.N. Combes, L. Zappia, P.X. Er, A. Oshlack, M.H. Little, Single-cell analysis reveals congruence between kidney organoids and human fetal kidney, Genome Med. 11 (1) (2019), https://doi.org/10.1186/s13073-019-0615-0.
[65] L.L. O'Brien, Q. Guo, E. Bahrami-Samani, J.-S. Park, S.M. Hasso, Y.-J. Lee, A. Fang, A.D. Kim, J. Guo, T.M. Hong, K.A. Peterson, S. Lozanoff, R. Raviram, B. Ren, B. Fogelgren, A.D. Smith, A. Valouev, A.P. McMahon, Transcriptional regulatory control of mammalian nephron progenitors revealed by multi-factor cistromic analysis and genetic studies, PLoS Genet. 14 (1) (2018), e1007181, https://doi.org/10.1371/journal.pgen.1007181.
[66] J. Xu, P.X. Xu, Eya-six are necessary for survival of nephrogenic cord progenitors and inducing nephric duct development before ureteric bud formation, Dev. Dynam. 244 (7) (2015) 866–873, https://doi.org/10.1002/dvdy.24282.
[67] L.L. O'Brien, Q. Guo, Y. Lee, T. Tran, J.D. Benazet, P.H. Whitney, A. Valouev, A. P. McMahon, Differential regulation of mouse and human nephron progenitors by the Six family of transcriptional regulators, Development 143 (4) (2016) 595–608, https://doi.org/10.1242/dev.127175.
[68] K. Hiratsuka, T. Monkawa, T. Akiyama, Y. Nakatake, M. Oda, S. Goparaju, H. Kimura, N. Chikazawa-Nohtomi, S. Sato, K. Ishiguro, S. Yamaguchi, S. Suzuki, R. Morizane, S. Ko, H. Itoh, M.S.H. Ko, Induction of human pluripotent stem cells into kidney tissues by synthetic mRNAs encoding transcription factors, Sci. Rep. 9 (1) (2019), https://doi.org/10.1038/s41598-018-37485-8.
[69] K.A. Kim, M. Wagle, K. Tran, X. Zhan, M.A. Dixon, S. Liu, D. Gros, W. Korver, S. Yonkovich, N. Tomasevic, M. Binnerts, A. Abo, R-Spondin family members regulate the Wnt pathway by a common mechanism, Mol. Biol. Cell 19 (6) (2008) 2588–2596, https://doi.org/10.1091/mbc.E08-02-0187.
[70] V.P. Vidal, F. Jian-Motamedi, S. Rekima, E.P. Gregoire, E. Szenker-Ravi, M. Leushacke, B. Reversade, M.C. Chaboissier, A. Schedl, R-spondin signalling is essential for the maintenance and differentiation of mouse nephron progenitors, Elife 9 (2020), e53895, https://doi.org/10.7554/eLife.53895.
[71] S. Boyle, T. Shioda, A.O. Perantoni, M. de Caestecker, Cited1 and Cited2 are differentially expressed in the developing kidney but are not required for nephrogenesis, Dev. Dynam. 236 (8) (2007) 2321–2330, https://doi.org/10.1002/dvdy.21242.
[72] S.P. Mah, H. Saueressig, M. Goulding, C. Kintner, G.R. Dressler, Kidney development in cadherin-6 mutants: delayed mesenchyme-to-epithelial conversion and loss of nephrons, Dev. Biol. 1 (1) (2000) 38–53, https://doi.org/10.1006/dbio.2000.9738, 223.
[73] M. Hochane, P.R. van den Berg, X. Fan, N. Bérenger-Currias, E. Adegeest, M. Bialecka, M. Nieveen, M. Menschaart, S.M. Chuva de Sousa Lopes, S. Semrau, Single-cell transcriptomics reveals gene expression dynamics of human fetal kidney development, PLoS Biol. 17 (2) (2019), e3000152, https://doi.org/10.1371/journal.pbio.3000152.
[74] D.R. Emlet, N. Pastor-Soler, A. Marciszyn, X. Wen, H. Gomez, W. Humphries, S. Morrisroe, J. Volpe, J.A. Kellum, Insulin-like growth factor binding protein 7 and tissue inhibitor of metalloproteinases-2: differential expression and secretion in human kidney tubule cells, Am. J. Physiol. Ren. Physiol. 312 (2) (2017) F284–F296, https://doi.org/10.1152/ajprenal.00271.2016.
[75] D. Chabardès-Garonne, A. Méjean, J.C. Aude, L. Cheval, A. Di Stefano, M. Gaillard, M. Imbert-Teboul, M. Wittner, C. Balian, V. Anthouard, C. Robert, B. Ségurens, P. Wincker, J. Weissenbach, A. Doucet, J.M. Elalouf, A panoramic view of gene expression in the human kidney, Proc. Natl. Acad. Sci. U. S. A 100 (23) (2003) 13710–13715, https://doi.org/10.1073/pnas.2234604100.
[76] S. Matsumoto, S. Fujii, A. Sato, S. Ibuka, Y. Kagawa, M. Ishii, A. Kikuchi, A combination of Wnt and growth factor signaling induces Arl4c expression to form epithelial tubular structures, EMBO J. 33 (2014) 702–718, https://doi.org/10.1002/embj.201386942.
[77] N. Pode-Shakked, R. Gershon, G. Tam, D. Omer, Y. Gnatek, I. Kanter, S. Oriel, G. Katz, O. Harari-Steinberg, T. Kalisky, B. Dekel, Evidence of in vitro preservation of human nephrogenesis at the single-cell level, Stem Cell Rep. 9 (1) (2017) 279–291, https://doi.org/10.1016/j.stemcr.2017.04.026.
[78] P. Wang, Y. Chen, J. Yong, Y. Cui, R. Wang, L. Wen, J. Qiao, F. Tang, Dissecting the global dynamic molecular profiles of human fetal kidney development by single-cell RNA sequencing, Cell Rep. 24 (13) (2018) 3554–3567, https://doi.org/10.1016/j.celrep.2018.08.056, e3.
[79] N. Miyamoto, M. Yoshida, S. Kuratani, I. Matsuo, S. Aizawa, Defects of urogenital development in mice lacking Emx2, Development 124 (9) (1997) 1653–1664, 10.1242/dev.124.9.1653. PMID: 9165114.
[80] S. Matsumoto, S. Fujii, A. Kikuchi, Arl4c is a key regulator of tubulogenesis and tumourigenesis as a target gene of Wnt–β-catenin and growth factor–Ras signalling, J. Biochem. 161 (1) (2017) 27–35, https://doi.org/10.1093/jb/mvw069.
[81] M. Narlis, D. Grote, Y. Gaitan, S.K. Boualia, M. Bouchard, Pax2 and Pax8 regulate branching morphogenesis and nephron differentiation in the developing kidney, J. Am. Soc. Nephrol. 18 (4) (2007) 1121–1129, https://doi.org/10.1681/ASN.2006070739.
[82] E.W. Brunskill, K. Georgas, B. Rumballe, M.H. Little, S.S. Potter, Defining the molecular character of the developing and adult kidney podocyte, PLoS One 6 (9) (2011), https://doi.org/10.1371/journal.pone.0024640.
[83] S. Sharmin, A. Taguchi, Y. Kaku, Y. Yoshimura, T. Ohmori, T. Sakuma, M. Mukoyama, T. Yamamoto, H. Kurihara, R. Nishinakamura, Human induced pluripotent stem cell-derived podocytes mature into vascularized glomeruli upon experimental transplantation, J. Am. Soc. Nephrol. 27 (6) (2016) 1778–1791, https://doi.org/10.1681/ASN.2015010096.
[84] R.I. Asfahani, M.M. Tahoun, E.V. Miller-Hodges, J. Bellerby, A.K. Virasami, R. D. Sampson, D. Moulding, N.J. Sebire, P. Hohenstein, P.J. Scambler, A.M. Waters,

Activation of podocyte Notch mediates early Wt1 glomerulopathy 93 (4) (2018) 903–920, https://doi.org/10.1016/j.kint.2017.11.014.
[85] R. Menon, E.A. Otto, A. Kokoruda, J. Zhou, Z. Zhang, E. Yoon, Y. Chen, O. Troyanskaya, J. Spence, M. Kretzler, C. Cebrián, Single-cell analysis of progenitor cell dynamics and lineage specification in the human fetal kidney, Development (Camb.) 145 (16 Special Issue) (2018), https://doi.org/10.1242/dev.164038.
[86] T. Tran, N.O. Lindström, A. Ransick, G. De Sena Brandine, Q. Guo, A.D. Kim, B. Der, J. Peti-Peterdi, A.D. Smith, M. Thornton, B. Grubbs, J.A. McMahon, A. P. McMahon, In vivo developmental trajectories of human podocyte inform in vitro differentiation of pluripotent stem cell-derived podocytes, Dev. Cell 50 (1) (2019) 102–116, https://doi.org/10.1016/j.devcel.2019.06.001, e6.
[87] M.S. Jae, C.T. Yu, K. Tang, T. Tanaka, T. Kodama, M.J. Tsai, S.Y. Tsai, The expression profiles of nuclear receptors in the developing and adult kidney, Mol. Endocrinol. 20 (12) (2006) 3412–3420, https://doi.org/10.1210/me.2006-0312.
[88] Lindström, N.O., De Sena Brandine, G., Tran, T., Ransick, A., Suh, G., Guo, J., Kim, A.D., Parvez, R.K., Ruffins, S.W., Rutledge, E.A., Thornton, M.E., Grubbs, B., McMahon, J.A., Smith, A.D., McMahon, A.P. Progressive recruitment of mesenchymal progenitors reveals a time-dependent process of cell fate acquisition in mouse and human nephrogenesis. Dev. Cell. 45(5): 651-660 doi: 10.1016/j.devcel.2018.05.010.
[89] T. Kitazawa, T. Sato, K. Nishiyama, R. Asai, Y. Arima, Y. Uchijima, Y. Kurihara, H. Kurihara, Identification and developmental analysis of endothelin receptor type-A expressing cells in the mouse kidney, Gene Expr. Patterns 11 (7) (2011) 371–377, https://doi.org/10.1016/j.gep.2011.04.001.
[90] F.A. Van den Brûle, P.L. Fernandez, C. Buicu, F.T. Liu, P. Jackers, R. Lambotte, V. Castronovo, Differential expression of galectin-1 and galectin-3 during first trimester human embryogenesis, Dev. Dynam. 209 (4) (1997) 399–405, https://doi.org/10.1002/(SICI)1097-0177(199708)209:4<399::AID-AJA7>3.0.CO;2-D.
[91] K. Aase, A. Abramsson, L. Karlsson, C. Betsholtz, U. Eriksson, Expression analysis of PDGF-C in adult and developing mouse tissues, Mech. Dev. 110 (1–2) (2002) 187–191, https://doi.org/10.1016/s0925-4773(01)00560-3.
[92] N.O. Lindström, J. Guo, A.D. Kim, T. Tran, Q. Guo, G. De Sena Brandine, A. Ransick, R.K. Parvez, M.E. Thornton, L. Baskin, B. Grubbs, J.A. McMahon, A. D. Smith, A.P. McMahon, Conserved and divergent features of mesenchymal progenitor cell types within the cortical nephrogenic niche of the human and mouse kidney, J. Am. Soc. Nephrol. 29 (3) (2018) 806–824, https://doi.org/10.1681/ASN.2017080890.
[93] A.R. England, C.P. Chaney, A. Das, M. Patel, A. Malewska, D. Armendariz, G. Hon, D. Strand, K. Drake, T.J. Carroll, Identification and characterization of cellular heterogeneity within the developing renal interstitium, Development (Cambridge, England) 147 (15) (2020), https://doi.org/10.1242/dev.190108.
[94] J. Yu, T.J. Carroll, J. Rajagopal, A. Kobayashi, Q. Ren, A.P. McMahon, A Wnt7b-dependent pathway regulates the orientation of epithelial cell division and establishes the cortico-medullary axis of the mammalian kidney, Development 136 (1) (2009) 161–171, https://doi.org/10.1242/dev.022087.
[95] G. Caruana, L. Cullen-McEwen, A.L. Nelson, X. Kostoulias, K. Woods, B. Gardiner, M.J. Davis, D.F. Taylor, R.D. Teasdale, S.M. Grimmond, M.H. Little, J.F. Bertram, Spatial gene expression in the T-stage mouse metanephros, Gene Expr. Patterns 6 (8) (2006) 807–825, https://doi.org/10.1016/j.modgep.2006.02.001.
[96] D.G. Matsell, P.J. Delhanty, O. Stepaniuk, C. Goodyear, V.K. Han, Expression of insulin-like growth factor and binding protein genes during nephrogenesis, Kidney Int. 46 (4) (1994) 1031–1042, https://doi.org/10.1038/ki.1994.364.
[97] K.S. Sastry, H. Naeem, Y. Mokrab, A.I. Chouchane, RNA-Seq reveals dysregulation of novel melanocyte genes upon oxidative stress: implications in vitiligo pathogenesis, Oxid. Med. Cell. Longev. (2019), 2841814, https://doi.org/10.1155/2019/2841814.
[98] A. Subramanian, E.H. Sidhom, M. Emani, K. Vernon, N. Sahakian, Y. Zhou, M. Kost-Alimova, M. Slyper, J. Waldman, D. Dionne, L.T. Nguyen, A. Weins, J. L. Marshall, O. Rosenblatt-Rosen, A. Regev, A. Greka, Single cell census of human kidney organoids shows reproducibility and diminished off-target cells after transplantation, Nat. Commun. 10 (2019) 5462, https://doi.org/10.1038/s41467-019-13382-1.
[99] A.N. Combes, B. Phipson, K.T. Lawlor, A. Dorison, R. Patrick, L. Zappia, R. P. Harvey, A. Oshlack, M.H. Little, Single cell analysis of the developing mouse kidney provides deeper insight into marker gene expression and ligand-receptor crosstalk, Development 146 (2019) 12, https://doi.org/10.1242/dev.178673, dev178673.
[100] T. Geuens, C.A. van Blitterswijk, V.L.S. LaPointe, Overcoming kidney organoid challenges for regenerative medicine, NPJ Regenerative Medicine 5 (2020) 8, https://doi.org/10.1038/s41536-020-0093-4.
[101] B.S. Freedman, Better being single? Omics improves kidney organoids, Nephron Clin. Pract. 141 (2) (2019) 128–132, https://doi.org/10.1159/000496009.
[102] S. Vukicevic, H.K. Kleinman, F.P. Luyten, A.B. Roberts, N.S. Roche, A.H. Reddi, Identification of multiple active growth factors in basement membrane matrigel suggests caution in interpretation of cellular activity related to extracellular matrix components, Exp. Cell Res. 1 (1992) 1–8, https://doi.org/10.1016/0014-4827(92)90397-Q.
[103] N.C. Talbot, T.J. Caperna, Proteome array identification of bioactive soluble proteins/peptides in Matrigel: relevance to stem cell responses, Cytotechnology 67 (5) (2015) 873–883, https://doi.org/10.1007/s10616-014-9727-y.
[104] T. Geuens, F.A.A. Ruiter, A. Schumacher, F.L.C. Morgan, T. Rademakers, L. E. Wiersma, C.W. van den Berg, T.J. Rabelink, M.B. Baker, V.L.S. LaPointe, Thiol-ene cross-linked alginate hydrogel encapsulation modulates the extracellular matrix of kidney organoids by reducing abnormal type 1a1 collagen deposition, Biomaterials 275 (2021), 120976, https://doi.org/10.1016/j.biomaterials.2021.120976.
[105] E. Garreta, P. Prado, C. Tarantino, R. Oria, L. Fanlo, E. Martí, D. Zalvidea, X. Trepat, P. Roca-Cusachs, A. Gavaldà-Navarro, L. Cozzuto, J.M. Campistol, J. C. Izpisúa Belmonte, C. Hurtado Del Pozo, N. Montserrat, Fine tuning the extracellular environment accelerates the derivation of kidney organoids from human pluripotent stem cells, Nat. Mater. 18 (4) (2019) 397–405, https://doi.org/10.1038/s41563-019-0287-6.
[106] Y. Zhu, L. Wang, F. Yin, Y. Yu, Y. Wang, H. Liu, H. Wang, N. Sun, H. Liu, J. Qin, A hollow fiber system for simple generation of human brain organoids, Integrative Biol. 9 (2017) 774–781, https://doi.org/10.1039/c7ib00080d.
[107] A. Kobayashi, K.M. Kwan, T.J. Carroll, A.P. McMahon, C.L. Mendelsohn, R. R. Behringer, Distinct and sequential tissue-specific activities of the LIM-class homeobox gene Lim1 for tubular morphogenesis during kidney development, Development 132 (12) (2005) 2809–2823, https://doi.org/10.1242/dev.01858.
[108] M.E. Melica, G. La Regina, M. Parri, A.J. Peired, P. Romagnani, L. Lasagni, Substrate stiffness modulates renal progenitor cell properties via a ROCK-mediated mechanotransduction mechanism, Cells 8 (12) (2019) 1561, https://doi.org/10.3390/cells8121561.
[109] M. Adam, A.S. Potter, S.S. Potter, Psychrophilic proteases dramatically reduce single-cell RNA-seq artifacts: a molecular atlas of kidney development, Development 144 (19) (2017) 3625–3632, https://doi.org/10.1242/dev.151142.
[110] J. Bejoy, Z. Wang, B. Bijonowski, M. Yang, T. Ma, Q.X. Sang, Y. Li, Differential effects of heparin and hyaluronic acid on neural patterning of human induced pluripotent stem cells, ACS Biomater. Sci. Eng. 4 (12) (2018) 4354–4366, https://doi.org/10.1021/acsbiomaterials.8b01142.
[111] B. Raphael, T. Khalil, V.L. Workman, A. Smith, C.P. Brown, C. Streuli, A. Saiani, M. Domingos, 3D cell bioprinting of self-assembling peptide-based hydrogels, Mater. Lett. 190 (2017) 103–106, https://doi.org/10.1016/j.matlet.2016.12.127.
[112] I. Chiesa, L. Cosimo, A.F. Bonatti, A. De Acutis, A.M. Smith, A. Saiani, G. Vozzi, C. De Maria, Modeling the three-dimensional bioprinting process of β-sheet self-assembling peptide hydrogel scaffolds, Frontiers in Med. Technol. 2 (2020), 571626, https://doi.org/10.3389/fmedt.2020.571626.
[113] A. Schumacher, M.B. Rookmaaker, J.A. Joles, R. Kramann, T.Q. Nguyen, M. van Griensven, V.L.S. LaPointe, Defining the variety of cell types in developing and adult human kidneys by single-cell RNA sequencing, NPJ Regenerative Medicine 6 (2021) 45, https://doi.org/10.1038/s41536-021-00156-w.
[114] L. Oxburgh, T.J. Carroll, O. Cleaver, D.R. Gossett, D.K. Hoshizaki, J.A. Hubbell, B. D. Humphreys, S. Jain, J. Jensen, D.L. Kaplan, C. Kesselman, C.J. Ketchum, M. H. Little, A.P. McMahon, S.J. Shankland, J.R. Spence, M.T. Valerius, J. A. Wertheim, O. Wessely, Y. Zheng, I.A. Drummond, (Re)Building a kidney, J. Am. Soc. Nephrol. 28 (5) (2017) 1370–1380, https://doi.org/10.1681/ASN.2016101077.
[115] R.R. Henry, J. Pettus, J. Wilensky, A.M.J. Shapiro, P.A. Senior, B. Roep, R. Wang, E.J. Kroon, M. Scott, K. D'Amour, H.L. Foyt, Initial clinical evaluation of VC-01TM combination product—a stem cell–derived islet replacement for type 1 Diabetes (T1D), Diabetes 67 (1) (2018), https://doi.org/10.2337/db18-138-OR.